Neurobiology of Disease

Heightened Hippocampal β-Adrenergic Receptor Function Drives Synaptic Potentiation and Supports Learning and Memory in the TgF344-AD Rat Model during Prodromal Alzheimer's Disease

Anthoni M. Goodman, Bethany M. Langner, Nateka Jackson, Capri Alex, and Lori L. McMahon
Department of Cell, Developmental, and Integrative Biology, University of Alabama at Birmingham, Birmingham, Alabama 35294-0006

The central noradrenergic (NA) system is critical for the maintenance of attention, behavioral flexibility, spatial navigation, and learning and memory, those cognitive functions lost first in early Alzheimer's disease (AD). In fact, the locus coeruleus (LC), the sole source of norepinephrine (NE) for >90% of the brain, is the first site of pathologic tau accumulation in human AD with axon loss throughout forebrain, including hippocampus. The dentate gyrus is heavily innervated by LC–NA axons, where released NE acts on β-adrenergic receptors (ARs) at excitatory synapses from entorhinal cortex to facilitate long-term synaptic plasticity and memory formation. These synapses experience dysfunction in early AD before cognitive impairment. In the TgF344-AD rat model of AD, degeneration of LC–NA axons in hippocampus recapitulates human AD, providing a preclinical model to investigate synaptic and behavioral consequences. Using immunohistochemistry, Western blot analysis, and brain slice electrophysiology in 6- to 9-month-old wild-type and TgF344-AD rats, we discovered that the loss of LC–NA axons coincides with the heightened β-AR function at medial perforant path–dentate granule cell synapses that is responsible for the increase in LTP magnitude at these synapses. Furthermore, novel object recognition is facilitated in TgF344-AD rats that requires β-ARs, and pharmacological blockade of β-ARs unmasks a deficit in extinction learning only in TgF344-AD rats, indicating a greater reliance on β-ARs in both behaviors. Thus, a compensatory increase in β-AR function during prodromal AD in TgF344-AD rats heightens synaptic plasticity and preserves some forms of learning and memory.

Key words: **Alzheimer's disease; β-adrenergic receptors; hippocampus; norepinephrine; TgF344-AD rat**

Significance Statement

The locus coeruleus (LC), a brain region located in the brainstem which is responsible for attention and arousal, is damaged first by Alzheimer's disease (AD) pathology. The LC sends axons to hippocampus where released norepinephrine (NE) modulates synaptic function required for learning and memory. How degeneration of LC axons and loss of NE in hippocampus in early AD impacts synaptic function and learning and memory is not well understood despite the importance of LC in cognitive function. We used a transgenic AD rat model with LC axon degeneration mimicking human AD and found that heightened function of β-adrenergic receptors in the dentate gyrus increased synaptic plasticity and preserved learning and memory in early stages of the disease.

Received Jan. 2, 2021; revised Feb. 23, 2021; accepted Apr. 28, 2021.

Author contributions: A.M.G., B.M.L., and L.L.M. designed research; A.M.G., B.M.L., N.J., and C.A. performed research; A.M.G. and B.M.L. analyzed data; A.M.G. and L.L.M. wrote the paper.

This work was supported by National Institutes of Health | National Institute of Neurological Disorders and Stroke (NINDS) Grant T32-NS-061788 (awarded to John Hablitz, University of Alabama at Birmingham in support of A.M.G.); National Institute on Aging grant R01 AG 0066489 and R21 053067 (awarded to LLM). We thank the University of Alabama at Birmingham Molecular Detection Core for use of reagents and tools for immunohistochemistry investigations. We also thank Dr. Karen Gamble for input on our statistical models, Dr. Christianne Strang for assistance in immunohistochemistry analysis, and Dr. Kavitha Abiraman for comments on the manuscript.

The authors declare no competing financial interests.

Correspondence should be addressed to Lori L. McMahon at mcmahon@uab.edu.

https://doi.org/10.1523/JNEUROSCI.0119-21.2021

Introduction

The locus coeruleus (LC) is the sole source of norepinephrine (NE) for >90% of the brain, and is critical for attention, behavioral flexibility, spatial navigation, and learning and memory (for review, see Poe et al., 2020). LC degeneration, predominantly caused by hyperphosphorylated tau (pTau) deposition (Braak et al., 2011; Arendt et al., 2015; Theofilas et al., 2017), is tightly associated with the transition from cognitively intact to amnestic mild cognitive impairment (aMCI; Braak et al., 2011; Arendt et al., 2015; Kelly et al., 2017; Theofilas et al., 2017) to dementia in Alzheimer's disease (AD) patients (Herrmann et al., 2004; Braak et al., 2011; Kelly et al., 2017). Though LC neurons can survive

for decades despite pTau accumulation (Kelly et al., 2017; Theofilas et al., 2018), their axons shorten, target regions are deafferented, and firing of LC neurons becomes destabilized (Chiodo et al., 1983; Booze et al., 1993; Gulyás et al., 2010). While amyloid-β (Aβ) induces neurotoxicity (Forest and Nichols, 2019), there are no reports of noradrenergic (NA) fiber degeneration in exclusively Aβ-expressing transgenic mouse models, suggesting that pTau accumulation is causal to NA fiber loss in human AD. Importantly, mimicking human NA degeneration in transgenic AD mice using the selective neurotoxin *N*-(2-chloroethyl)-*N*-ethyl-2-bromobenzylamine hydrochloride enhances Aβ plaque deposition (Heneka et al., 2006; Jardanhazi-Kurutz et al., 2011), neuroinflammation (Heneka et al., 2002; Pugh et al., 2007), and cognitive/behavioral deficits (Jardanhazi-Kurutz et al., 2010; Rey et al., 2012). Furthermore, loss of NA tone can enhance the sensitivity of adrenergic receptors (ARs) to agonist activation, known as "denervation supersensitivity" (Deguchi and Axelrod, 1973; Bannister et al., 1981; Dooley et al., 1983; Monti et al., 1988), which is believed to result from increased receptor expression, and is present in human AD (Deguchi and Axelrod, 1973; Kalaria et al., 1989a). However, the consequences of this AR supersensitivity are unknown.

In contrast to transgenic mouse models harboring human Aβ mutations, the TgF344-AD rat with APP_{swe} and $PS1_{\Delta E9}$ mutations has endogenous pTau deposition in LC early in the disease (Cohen et al., 2013; Rorabaugh et al., 2017). Reductions in NA fiber density, which is accompanied by deficits in cognitive flexibility measured by reversal learning (Rorabaugh et al., 2017), occur in the entorhinal cortex (EC) and dentate gyrus (DG) by 16 months of age. Importantly, this cognitive deficit is rescued by enhancing LC activity using chemogenetic activation, further confirming a critical role of the LC–NA system in maintaining cognitive function in AD.

The DG is the gatekeeper for the hippocampus, and is critical for learning and memory (Patrylo and Williamson, 2007; Dengler and Coulter, 2016). The DG contains the highest NA fiber density and expression of β_1-ARs and β_2-ARs in the hippocampal formation (Loy et al., 1980; Nicholas et al., 1993). β-ARs in the DG facilitate both long-term potentiation (LTP) and long-term depression (LTD), depending on the salience of the experience, simultaneous with enhancing learning, all of which are prevented by pharmacological blockade of β-ARs (O'Dell et al., 2015; Hagena et al., 2016; Hansen, 2017). In human AD, excitatory inputs from the EC to DG malfunction first (Khan et al., 2014). Importantly, using the TgF344-AD rat model, we previously found that altered synaptic function, including enhanced LTP, appears first at medial perforant path (MPP) synapses from the EC onto dentate granule cells (DGCs) mimicking the early dysfunction in human AD.

Here, in TgF344-AD rats, we found reduced hippocampal NA axon density beginning at 6 months of age, which is considerably earlier than first reported (Rorabaugh et al., 2017). In synaptic physiology studies at time points when NA axon loss is significant, we discovered heightened β-AR function at MPP–DGC synapses that is mechanistically linked with the heightened LTP magnitude we previously reported (Smith and McMahon, 2018). Importantly, this heightened β-AR function facilitates novel object recognition (NOR) in TgF344-AD rats and enables fear extinction learning, thereby providing a possible mechanism to explain how cognitive abilities are protected in the prodromal stage of AD. Understanding how the NA system changes in early or prodromal AD opens the door for innovative therapies and a more comprehensive view of neurodegenerative disorders impacting the LC–NA system.

Materials and Methods

Animals

A total of 280 male and female TgF344-AD rats harboring the human Swedish amyloid precursor protein (APP_{swe}) and δ exon 9 mutant presenilin-1 ($PS1_{\Delta E9}$) were bred with nontransgenic F344 females [Envigo (previously Harlan Laboratories)] at the University of Alabama at Birmingham. All breeding and experimental procedures were approved by the University of Alabama Institutional Animal Care and Use Committee and follow guidelines set by the National Institutes of Health. The original breeding pair was obtained from Terrence Town (University of Southern California, Los Angeles, CA; Cohen et al., 2013). Rats were maintained under standard animal care facility conditions with food (catalog #Harlan 2916, Teklad Diets) and water *ad libitum* and a 12 h light/dark cycle at 22°C and 50% humidity. Rats used for behavioral assays were reverse light entrained for a minimum of 2 weeks. Rats were housed in standard rat cages (height, 7 inches; floor area, 144 square inches) in same-sex groups of four or less at weights of ~300 g or two per cage when ≥400 g. Rats were aged from birth to experimental age groups not exceeding 24 months. Because of colony restrictions, only male rats were used for immunohistochemistry (IHC; age range, 3–24 months) and brain slice electrophysiology experiments using dendritic field potential recordings (age range, 9–10 months; see Figs. 2*A1–B2*, 3). Both male and ovariectomized female (>2 weeks before experimentation to avoid modulation of synaptic plasticity by estrous cycle changes) rats were used for calcium channel experiments (age range, 9–10 months), behavior (age range, 10–13 months), biochemistry (age, 9–11 months), and LTP experiments (age, 6 months). In our previous report (Smith and McMahon, 2018), we found no differences in synaptic transmission and plasticity between sexes at these ages.

Genotyping

The presence of transgenes was verified twice for each animal, first using ear punches (collected at postnatal day 21) and again using cerebellar tissue collected on the day the animal was killed. APP_{swe} and $PS1_{\Delta E9}$ transgene expression were confirmed using PCR and the Terra PCR Direct Polymerase Mix (Clontech Laboratories). PCR cycling parameters, primers, and analyses followed those of (Smith and McMahon, 2018). Animals were excluded from the study if their PCR genotyping did not match or was ambiguous.

Immunohistochemistry

Serial coronal sections containing dorsal hippocampus were cut (50 µm) from transcardially perfused and PFA-fixed hemispheres (vibratome VT1000P, Leica; from 3-, 6-, 9-, 12-, 15-, 19-, and 24-month-old animals) and stored in individual wells with 0.1 M PBS plus 0.04% Na-azide. Dorsal hippocampal sections were washed in 0.01 M PBS, pH 7.2, before blocking endogenous peroxidase activity with 3% H_2O_2 in 0.01 M PBS for 10 min and washed again two more times. Nonspecific binding sites were blocked by incubating sections in PBS blocking buffer (1% bovine serum albumin, 0.2% nonfat powdered skim milk, 0.3% Triton X-100, filter sterilized) for 60 min at room temperature. Sections were incubated in anti-tyrosine hydroxylase (TH) polyclonal antibody (Ab; 1:100; stock #ab152, EMD Millipore) or anti-Aβ (1:400; stock #6E10) for 18 h. TH fibers in hippocampus have been found to colocalize with dopamine β-hydroxylase-positive fibers (Moudy et al., 1993) serving as a homolog for noradrenergic fiber labeling. Primary-labeled slices were washed in 0.01 M PBS 6× 10 min and then incubated with 1:100 Alexa Fluor 564 Dk-a-ms or Alexa Fluor 564 Dk-a-rb for 2 h. Slices were washed again, mounted (Fisherbrand Superfrost Plus Slides, Thermo Fisher Scientific), and coverslipped in Fluoromount with DAPI.

Confocal microscopy

Labeled slices were imaged with a confocal laser-scanning microscope (model A1R, Nikon) equipped with a high-definition multichannel detector for RGB and far red imaging with balanced emissions at 405, 488, 561, and 640 nm. To obtain an optimal signal-to-noise ratio for each fluorophore, we adjusted the gain and offset on a slide containing positively labeled tissue in parallel followed by taking the mean fluorescence/pixel of two sequential scans. Adjustments were made in the dedicated

interface with NIS Elements C. Regions of interest [dentate gyrus (within the hilus), CA3, and CA1] were imaged, acquiring 22–26 stacks of 0.225 μm increments at 40× magnification. One series of slices was labeled in parallel without the addition of primary antibodies to be used as a negative control (data not shown).

Image processing

Digitized images were processed using FIJI (FIJI is just ImageJ, 2015) in which images were split by color channel, and these channels processed individually for quantification purposes. Twenty digital sections (each section being 0.225 μm in the *z*-direction) were collapsed into a *z*-projection by average pixel intensity. Brightness/contrast intensity was universally changed to exclude oversaturated or undersaturated pixels. DAPI images were used to create regions of interest that fell into the crux of CA3, stratum radiatum of CA1, and the hilar region of the dentate gyrus. TH-immunostained images were then analyzed with a standardized segmentation plugin, WEKA (Schindelin et al., 2012; Arganda-Carreras et al., 2017; University of Waikato, Hamilton, New Zealand). This plugin uses an ideal image (approximately average signal/noise ratio) chosen to represent a mean distribution of pixel values (fluorescent signal) to create a single fast-random-forest classifier by machine learning. The classifier generated from several training iterations is then applied to the rest of the dataset to segment "objects" (in this case, TH^+ fibers), which were extracted for further analysis. These extracted TH^+ fiber images were made binary, and objects of <10 pixels (~3.14 μm) were removed. A standard FIJI analysis tool, "Classify Particles Using Skeleton" was used to measure the length and area of the segmented objects. The "cutoff/snapto distance" of 30 pixels was used to fill small gaps missed by the segmentation tool. These results were expressed as a length per area (based on the region of interest). A total of two collapsed stacks per subfield (DG, CA3, CA1), per rat were imaged and underwent image processing. The total length per area, per rat, were averaged for statistical analyses.

Hippocampal slice preparation

Rats, 6 or 9–10 months of age, were anesthetized via deep isoflurane inhalation and rapidly decapitated, and brains were removed. Coronal slices (400 μm) from dorsal hippocampus were prepared using a vibratome (model VT1000P, Leica). Slices were made in low Na^+, sucrose-substituted ice-cold artificial CSF (aCSF) containing (in mM): NaCl 85, KCl 2.5, $MgSO_4$ 4, $CaCl_2$ 0.5, NaH_2PO_4 1.25, $NaHCO_3$ 25, glucose 25, and sucrose 75, saturated with 95% O_2, 5% CO_2, at pH 7.4. Slices were held in a water bath at 26°C for 1 h in standard aCSF containing the following (in mM): 119.0 NaCl, 2.5 KCl, 1.3 $MgSO_4$, 2.5 $CaCl_2$, 1.0 NaH_2PO_4, 26.0 $NaHCO_3$, and 11.0 glucose, saturated with 95% O_2, 5% CO_2, at pH 7.4 before transfer to the submersion chamber for recordings.

Electrophysiology

Extracellular dendritic field EPSPs (fEPSPs) were recorded from DGCs from stimulation to the MPP in a submersion chamber continuously perfused with standard aCSF warmed to 26.5–28.5°C. Baseline fEPSPs were generated by stimulating the MPP input onto DGCs (0.1 Hz for 200 μs) using a twisted insulated nichrome wire (A-M Systems) electrode placed in MPP within 200–300 μm of an aCSF-filled glass recording electrode. Correct electrode placement was verified visually and by the generation of paired-pulse depression, a characteristic of the MPP–DGC synapses (McNaughton and Barnes, 1977; Smith and McMahon, 2018), at an interstimulus interval of 50 ms through the duration of the experiment. Baseline fEPSPs were obtained at ~50% maximal response (~0.5 mV in amplitude) and experiments with ≥8% variance in baseline were not included in the final datasets. Rats were interleaved by genotype for any given dataset to control for technical artifacts. Bath application of drugs [NE or isoproterenol (ISO), for 10 min] followed the collection of a stable 20 min baseline.

Long-term potentiation

High-frequency stimulation (HFS; four trains of 100 Hz, for 500 ms, separated by 20 s) was used to induce LTP at the MPP–DGC synapses and used a platinum/iridium bipolar stimulating electrode (FHC). Strong inhibition of DGCs greatly reduces HFS-driven LTP at MPP–DGC synapses (Coulter and Carlson, 2007; Smith and McMahon, 2018), which necessitates $GABA_A$ receptor ($GABA_AR$) antagonism to allow sufficient postsynaptic depolarization to relieve the Mg^{2+} block from NMDARs. Therefore, picrotoxin (100 μM) was included in the bath solution to inhibit $GABA_ARs$ for the duration of the experiment. A 20 min stable baseline was collected before HFS at 1.5× baseline stimulation amplitude. The NMDAR-dependent HFS protocol includes four trains of 100 Hz for 500 ms, with each sweep separated by 20 s. A partial block of β-ARs was accomplished with 1 μM propranolol (PROP), which was present in the bath for the duration of the experiment. Experiments for each condition—genotype by treatment—were interleaved to control for technical artifact.

Whole-cell voltage clamp

Slices were allowed to recover for 60 min following slicing and transferred to a submersion chamber continuously perfused with modified aCSF as follows (in mM): 100.0 NaCl, 2.5 KCl, 1.3 $MgSO_4$, 2.5 $CaCl_2$, 1.0 NaH_2PO_4, 26.0 $NaHCO_3$, 11.0 glucose, 25 tetraethylammonium chloride, 0.01 6,7-dinitroquinoxaline-2,3-dione, 0.005 3-(2-carboxypiperazin-4-yl)propyl-1-phosphonic acid, and 0.1 picrotoxin, saturated with 95% O_2, 5%CO_2, at pH 7.4 and held at 28.0 ± 0.4°C. A dissecting microscope was used to target the cell layer of the dentate gyrus, and DGCs were blind patched. Electrodes [2–6 MΩ; filled with the following (in mM): 120 cesium gluconate, 0.6 EGTA, 5 $MgCl_2$, 2 ATP, 0.3 GTP, 20 HEPES, and 5 QX-314 *N*-(2,6-dimethylphenylcarbamoylmethyl) triethylammonium bromide, at pH 7.21 and 306 mOsm] were used to patch DGCs of the dorsal hippocampus. DGCs were held at −80 mV and underwent a 20 ms hyperpolarizing step (−100 mV) followed by 5 mV steps from −60 to +35 mV for 50 mS, with sweeps occurring every 5 s. Pilot experiments showed a robust rundown of calcium currents that occurred within several minutes, as previously reported (Doroshenko et al., 1982; Murchison and Griffith, 1996). This necessitated the experiment to be run immediately following break-in. To avoid ISO-induced β-AR endocytosis,recordings were terminated following 20 min of ISO exposure (Wang et al., 2011).

Pharmacology

All drugs for electrophysiology were made into stock solutions and stored at −20°C or 4°C according to manufacturer recommendations and mixed to working concentration in aCSF immediately before use. NE (stock solution, 4 mM; working solution, 40 μM), PROP (stock solution, 10 mM; working solution, 10 μM), metoprolol (Met; stock solution, 20 mM; working solution, 20 μM), ISO (stock solution, 20 mM; working solution, 1 or 10 μM) were purchased from Sigma-Aldrich. ICI 118,551 (ICI; stock solution, 10 mM; working solution, 300 nM) was purchased from Tocris Bioscience. Propranolol used for behavioral assays was made fresh in sterile saline (0.676 mM).

Western blot

To investigate β-AR signaling, hippocampal slices were prepared similarly to those in electrophysiology experiments. The DG was subdissected and allowed to recover for 1 h in oxygenated aCSF with kyneurinic acid (2 mM) to reduce activity in the slice, which could modulate the basal phosphorylation of extracellular signal-regulated kinase (ERK). Subdissected slices were assigned to control or treatment with ISO (1 μM; via bath application) for 30, 60, or 120 s followed by immediate flash freezing in liquid N2. Tissues were later homogenized in a buffer containing protease and phosphatase inhibitors, and centrifuged at 25,000 × *g* for 15 min, and lysates were removed. Lysates were evaluated by ELISA and subsequently diluted to 30 μg/well. Western blots all contained two ladders and three control lanes, total protein was labeled, and measured via fluorescent scanning before 1^0 Ab application. The 1^0 Abs include ERK, phospho-ERK (pERK), GluA1(pS845), GluA1, and GAPDH. All Western blots were run in duplicate, and the average concentration of the duplicates was used. Phospho-ERK was divided by total ERK (i.e., pERK42/ERK42), and all values were divided by total protein. GAPDH values were used to verify the total protein per lane. Control lanes were averaged and used for comparison across blots.

Cannula surgery

Eighty-one rats underwent cannulation surgery targeting the lateral ventricles at 9–11 months of age. Rats were anesthetized with isoflurane and a guide cannula [3 mm; catalog #C232G-3.0/SPC, P1 Technologies (formerly Plastics One)] with dummy (+1 mm projection, C232G-3.0) was installed at −0.75 anteroposterior and ±1.5 mediolateral from bregma. The cannula was fixed in place with dental cement and anchored into the skull with four screws. To confirm the correct placement of the cannula, a dye (Fast Green FCF, Sigma-Aldrich) was infused into the cannula following behavioral assay completion. The detection of dye in the ventricles was used to verify appropriate placement following behavioral assay completion.

Behavior

Novel object recognition. Ten- to 13-month-old rats were reverse light entrained for a minimum of 2 weeks, during which they were handled every other day for 5 min to socialize them for eventual infusions. Rats were bilaterally infused intracerebroventricularly (5 µl/hemisphere at a rate of 1 µl/min) each day of the 3 d of the NOR task 30 min before behavior and were placed in the NOR box for 5 min. Rats received saline infusions on days 1 and 3. On day 1, rats were habituated to the empty NOR box (length × width × height: 60 × 41 × 40 cm). Day 2 served as the learning day in which two identical objects (similarly sized and shaped silicone rubber bear- or squirrel-shaped dog toys) were placed equidistant (11 cm) from the sides of the box, and the rats were infused with either 2 µg of PROP in saline or with the saline vehicle alone. This concentration was chosen based on previous studies in the literature (Kemp and Manahan-Vaughan, 2008) with the goal of a partial blockade of β-ARs without changing basal synaptic transmission or interfering with learning in wild-type control rats. The goal of infusion on day 2 was to determine whether TgF344-AD rats are more reliant on β-AR enhancement of learning to recognize the identical objects. On day 3, one of the objects is replaced with a very differently shaped silicone rubber dog toy (a hoagie), and the rat was tasked to spend more time with the novel object. The use of bears/squirrels, treatment type, and side of the box in which the novel object replaced a familiar object was interleaved by genotype. No side or object preferences were detected. All personnel were blinded to genotype and treatment during the experiment and the analysis. Behavior was analyzed using Noldus EthoVision, and the investigation of objects was manually scored by at least two trained researchers. Investigative behaviors were defined as the nose of the rat contacting or both being within 2 cm and directed at the object or front paw contact with the object. Rats that interacted for <1 s with each object on day 2 or those with no interaction on day 3 were excluded on the basis of nonparticipation. The number of rats excluded from analyses were not different between groups based on an ANOVA ($F_{(3,77)} = 0.7326$, $p = 0.5357$).

Contextual fear conditioning. A week following NOR, the same rats underwent contextual fear conditioning and extinction learning, receiving the same treatment condition as they had in the NOR task. Contextual fear conditioning was performed in a custom operant conditioning box (29.53 × 23.5 × 20.96 cm) over 4 d with a goal of generating a fear memory and determining whether the TgF344-AD rats rely on β-ARs for fear extinction learning. Here the box served as the context with an associated fear memory (shock). Rats received an infusion of PROP or vehicle on days 2, 3, and 4, 30 min before being placed in the box. On day 1, which serves as the baseline for exploratory and nonfreezing behavior, the rat was allowed to explore the box for 7 min, then received three shocks (0.5 mA for 1 s with 1 min intervals) and was immediately removed from the box. On days 2, 3, and 4, rats were placed in the box for 5 min and did not receive a shock. Freezing activity was video recorded (Video Freeze, Med Associates) during each session. Time spent freezing was divided by the total time in the box to generate a percentage of time spent freezing per day. To measure fear extinction learning, rats were required to adequately recall the fear association on day 2 by spending >30% of their time frozen. To this end, excluded animals included the following: WtV (Wt +Vehicle), 3 of 24 (12.5%); WtP (Wt+ Propranolol), 6 of 25 (24%); TgV (Tg+Vehicle), 3 of 15 (20%); and TgP (Tg+ Propranolol), 5 of 15 (33%). A χ^2 test of independence showed that there was no significant association between the numbers of rats excluded and experimental group ($\chi^2_{(3,80)} = 2.476$, $p = 0.480$).

Experimental design and statistical analyses

Age was not interleaved, therefore all statistical analyses for each experiment were performed within each experimental cohort (e.g., 6-month-old male TgF344-AD rat vs non-Tg littermate) and not across cohorts. Results were reported as the mean ± SEM with significance set at $p < 0.05$ (*) determined by unpaired Student's t test assuming unequal variance, and repeated measures of general linear models, typically one-way or two-way repeated-measures ANOVA. Multiple comparisons were determined a priori and underwent Bonferroni's or Dunnett's correction when values were only compared with a control. Survival analyses are reported as χ^2. Manual behavior scores were compared by cohort and object with a Pearson's R to verify interrater reliability > 0.80 (mean ± SD $r = 0.908 \pm 0.061$). Non-normally distributed small samples were evaluated using an independent samples Kruskal–Wallis test of the median. Statistical analysis was performed using Prism 7 (GraphPad Software) and SPSS 26 (IBM). All graphs were created in Prism 7. Sufficient power was determined with G*Power 3.1.9.2 (Franz Faul, University Kiel, Germany). Electrophysiological data were acquired using Clampex 10.6 or 10.7 (pClamp; Molecular Devices) and analyzed offline in Clampfit 10.6 or 10.7 (Molecular Devices). For extracellular recordings, the n represents the number of animals; when more than one slice was used in experiments from a single animal, the data were averaged to represent that animal. For whole-cell recordings, the n represents the number of cells and N represents the number of animals.

Results

Pathologic changes begin at 6 months in the hippocampus of the TgF344-AD rat

Previous reports show Aβ plaque development in TgF344-AD rats as early as 6 months (Cohen et al., 2013; Rorabaugh et al., 2017). Using IHC with the anti-Aβ antibody 6E10, we created a time course of Aβ plaque deposition in serial coronal sections from male TgF344-AD and nontransgenic [wild-type (WT)] littermates. Consistent with the study by Rorabaugh et al. (2017), we found small plaques in the hilus of the DG (Fig. 1*A*, arrow) as early as 6 months with large, mature plaques visible by 9 months that persisted with age. Two-way repeated-measures (RM) ANOVA confirmed a significant interaction of genotype and age in DG and CA1 [DG: $F_{(4,30)} = 2.62$, $p = 0.054$ (Fig. 1*A*); CA1: $F_{(4,30)} = 2.96$, $p = 0.036$ (data not shown)]. Two-way RM ANOVA in CA3 yielded a significant effect of genotype ($F_{(1,30)} = 9.30$, $p = 0.005$) but not age ($p > 0.05$, data not shown).

Significant accumulation of pTau has been reported in LC of TgF344-AD rats beginning at 6 months of age, with significant loss of dopamine β-hydroxylase-positive NA fibers (DβH$^+$) in dentate gyrus at 16 months of age, but not at 6 months of age (Rorabaugh et al., 2017). To detail the time course of LC axon degeneration in hippocampus during early disease progression and before reported significant memory loss (Rorabaugh et al., 2017), we used anti-TH IHC to identify NA axons and found that TH$^+$ fiber density was reduced across the hippocampus in TgF344-AD rats [two-way RM ANOVA; DG: $F_{(1,37)} = 10.30$, $p = 0.003$ (Fig. 1*B*); CA1: $F_{(1,37)} = 8.14$, $p = 0.007$; CA3: $F_{(1,37)} = 18.75$, $p = 0.0001$ (data not shown)]. Planned comparisons demonstrated significant reductions of TH$^+$ fiber density beginning at 6 months (DG: $t_{(6)} = 2.82$, $p = 0.03$; CA1: $t_{(6)} = 2.62$, $p = 0.040$; 57% in CA3: $t_{(6)} = 3.65$, $p = 0.011$) in contrast to no differences between genotype at 3 months of age [DG: $t_{(6)} = 0.12$, $p = 0.91$ (Fig. 1*B*); CA1: $t_{(6)} = 0.81$, $p = 0.45$; CA3: $t_{(6)} = 0.83$, $p = 0.44$ (data not shown)]. These findings suggest that NA denervation begins as early as 6 months of age in the TgF344-AD rat.

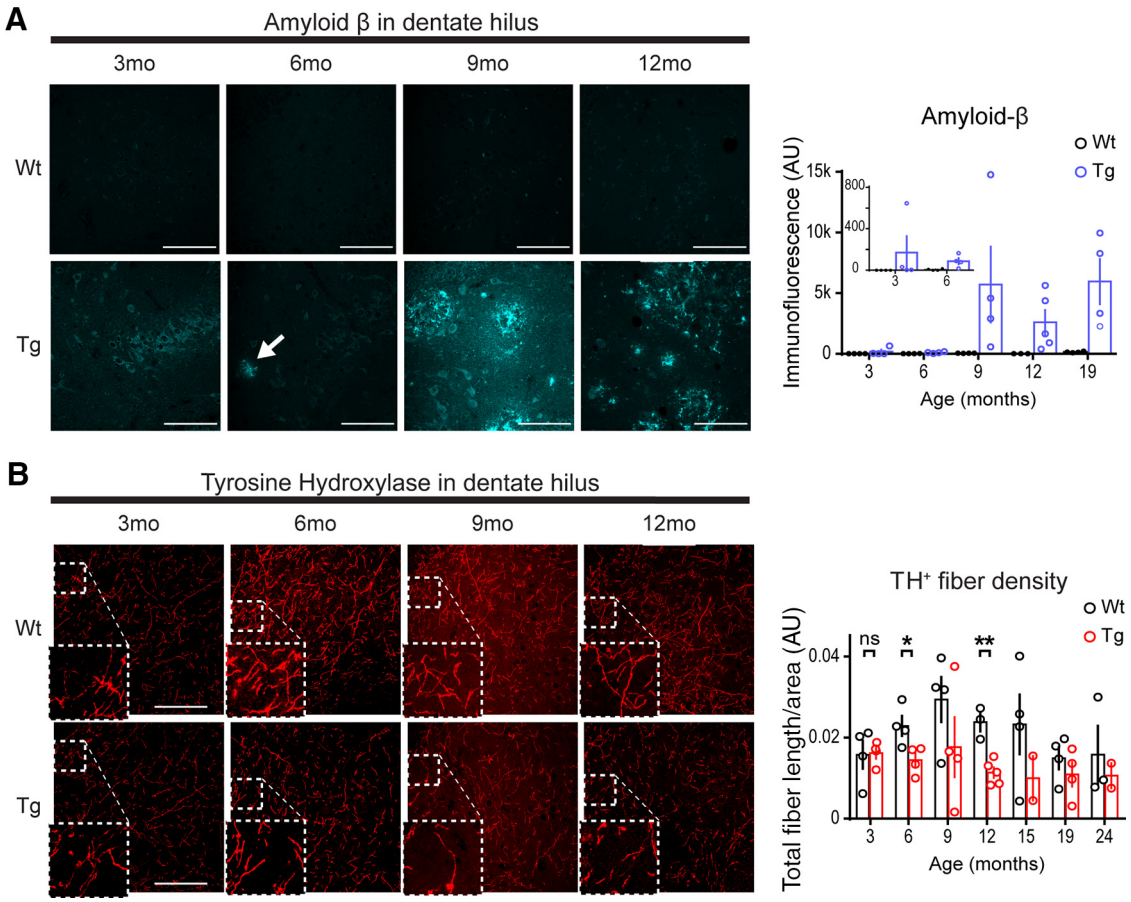

Figure 1. Aβ accumulation and tyrosine hydroxylase fiber loss first detected at 6 months of age in hippocampus of the TgF344-AD rat. ***A***, Representative images of anti-Aβ (6E10 Ab) in WT and Tg DG hilus of male rats at 3 (WT, $n = 4$; Tg, $n = 4$), 6 (WT, $n = 4$; Tg, $n = 4$), 9 (WT, $n = 4$; Tg, $n = 4$), and 12 (WT, $n = 3$; Tg, $n = 5$) months of age. Small, dispersed, immunopositive plaques appear at 6 months of age (arrow) and appear more commonly, and larger at later months of age in Tg rats. Scale bars, 100 μM. Bar graph (right) of quantified total immunofluorescence, including 19-month-old male rats (WT, $n = 4$; Tg, $n = 4$) was significant for the interaction of genotype and age ($p = 0.05$). ***B***, Representative images of anti-TH (ab152) in DG from the same WT and Tg rats at 3, 6, 9, and 12 months of age. Insets, enlarged regions where outlined. Scale bars, 100 μM. Bar graph (right) of total fiber length/area arbitrary units (AU) including 15- (WT, $n = 4$; Tg, $n = 2$), 19- (WT, $n = 4$; Tg, $n = 4$), and 24-month-old male rats (WT, $n = 3$; Tg, $n = 2$) was significant for genotype differences ($p < 0.01$), but not age ($p > 0.1$). Fiber density was not different between genotypes at 3 months ($p > 0.1$), but is at 6 months ($p < 0.05$) and 12 months ($p < 0.01$). All values are the mean ± SEM. ns, not significant. *$p \leq 0.05$, **$p \leq 0.01$.

Pharmacological activation of β-ARs induces heightened synaptic potentiation at MPP–DGC synapses in TgF344-AD rats

Loss of NA innervation can lead to heightened function of ARs, a phenomenon referred to as "denervation supersensitivity" (Deguchi and Axelrod, 1973; Bannister et al., 1981; Dooley et al., 1983; Monti et al., 1988). Therefore, we tested whether AR function is indeed increased in Tg-F344-AD rats when NA axon degeneration is significant by asking whether the modulation of synaptic strength is increased following agonist application. We chose 9-month-old rats since TH^+ axon loss is significant at this age, and we used NE (40 μM) to mimic the actions of endogenous neurotransmitter at ARs. Bath-applied NE (40 μM) during fEPSP recordings elicited a long-term potentiation of the fEPSP at MPP–DGC synapses in slices from TgF344-AD rats, measured 40 min after NE washout compared with baseline ($t_{(9)} = 2.343$, $p = 0.044$), and was not different between genotypes ($t_{(16)} = 0.079$, $p = 0.94$; Fig. 2*A1*). However, the time to peak potentiation of the fEPSP slope, estimated by survival analysis, was much shorter in TgF344-AD rats (log-rank Mantel–Cox test) $\chi^2_{(1,18)} = 8.88$, $p = 0.003$ (Fig. 2*A2*), suggesting an enhanced response to NE in the TgF344-AD rats. Because β-AR activation potentiates basal transmission and facilitates LTP induction at MPP–DGC synapses (Pelletier et al., 1994; Lethbridge et al., 2014; O'Dell et al., 2015; Hagena et al., 2016), we asked whether β-AR activation underlies the effects of exogenous NE application. Pretreatment with the β-AR-selective antagonist PROP (10 μM) abolished the long-lasting synaptic potentiation in both genotypes (TgF344-AD: $t_{(8)} = 0.42$, $p = 0.69$; WT: $t_{(7)} = 0.060$, $p = 0.9562$) and completely eliminated the faster time to peak fEPSP potentiation in TgF344-AD rats ($\chi^2_{(1,17)} = 0.066$, $p = 0.80$; Fig. 2*B1*,*B2*), confirming a role of β-ARs in maintaining NE-induced long-lasting potentiation and suggesting enhanced function of β-AR as causal to faster time to peak in the TgF344-AD rats.

β-AR activation alone is sufficient to induce heightened potentiation at MPP–DGC synapses in TgF344-AD rats

To determine whether β-AR activation is sufficient to cause synaptic potentiation at MPP–DGC synapses in TgF344-AD rats, we used the selective β-AR agonist ISO (Fig. 3*A*,*B*). While bath application of ISO (10 μM) produced a potentiation similar in magnitude in TgF344-AD and WT rats ($t_{(9)} = 0.030$, $p = 0.978$), unexpectedly, we found no difference in the time to peak potentiation (log-rank Mantel–Cox test: $\chi^2_{(1,10)} = 1.150$, $p = 0.28$) between TgF344-AD rats and WT, contrary to observations following NE application. We postulated that the more rapid onset

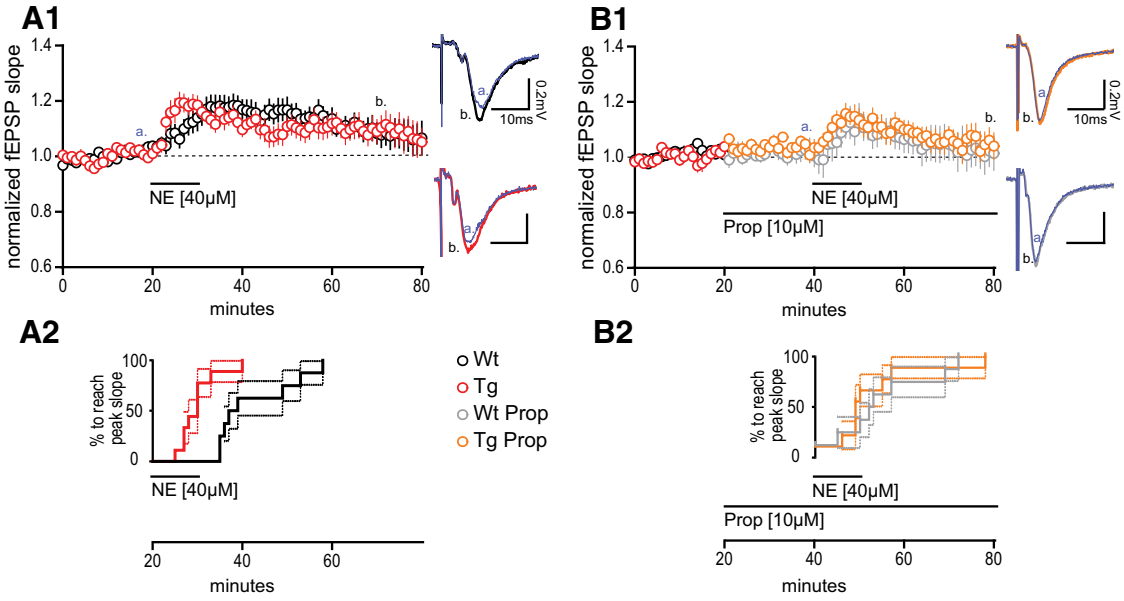

Figure 2. Heightened synaptic potentiation at MPP–DGC synapses in TgF344-AD rats induced by norepinephrine requires β-adrenergic receptors. ***A1***, NE (40 μM) was bath applied during extracellular dendritic field potential recordings at MPP–DGC synapses in slices from 9- to 10-month-old Tg ($n = 10$) and WT ($n = 8$) rats. Representative averaged fEPSP traces (five sweeps) from WT (black) and Tg (red). Calibration: 0.2 mV, 10 mS at times *t* [a = 20 min (blue); b = 60 min]. Long-term potentiation was reached for Tg fEPSPs at *t*(65–70), 40 min following NE washout ($p < 0.05$), and was not different between genotypes ($p > 0.1$). ***A2***, Survival analysis plot displaying the time at which the fEPSP in each slice reaches peak potentiation, demonstrating a significantly more rapid time to peak in Tg compared with WT ($p < 0.001$). ***B1***, ***B2***, The β-AR antagonist PROP (10 μM) prevents the rapid increase in synaptic potentiation in Tg rats ($p > 0.1$; ***B2***), and blocks the long-lasting potentiation in both genotypes from *t*(35–40) to *t*(75–80) of Tg ($n = 9$) and WT ($n = 8$) when compared with paired *t* tests (both, $p > 0.1$). Representative traces for WT + PROP (gray) and Tg + PROP (orange) with calibration (0.2 mV, 10 mS) at times *t* (a = 40 min; b = 80 min). All values are the mean ± SEM.

of potentiation in the TgF344-AD rats could be masked by higher affinity and more rapid β-AR activation by ISO compared with NE (Swaminath et al., 2004). Thus, we considered that a threshold, 10-fold lower concentration of ISO (1 μM) might reveal a difference between TgF344-AD rats and WT. Consistent with the heightened function of β-ARs at MPP–DGC synapses in TgF344-AD rats, we observed a statistically greater magnitude potentiation during and after ISO application (20–70 min) in the TgF344-AD rats compared with WT (two-way RM $ANOVA_{20\text{-}70min}$ ($F_{(1,13)} = 5.60$, $p = 0.034$; Fig. 3*B*).

Because both β_1-ARs and β_2-ARs are present in DG and can have distinct and overlapping roles in the modulation of neural circuits (Gibbs and Summers, 2002; Kemp and Manahan-Vaughan, 2008), we selectively blocked them to determine which subtype is driving the synaptic potentiation. The selective β_2-antagonist ICI 118,551 (300 nM) did not prevent the ISO-induced potentiation of fEPSPs in TgF344-AD rats compared with WT at either ISO concentration (Fig. 3*C*,*D*; 10 μM; two-way RM $ANOVA_{40\text{-}60min}$ interaction: $F_{(20,120)} = 2.21$, $p = 0.005$; 1 μM; two-way RM $ANOVA_{40\text{-}60min}$ time: $F_{(20,160)} = 3.74$, $p < 0.0001$). However, the selective β_1-antagonist metoprolol (20 μM) completely abolished the ISO-induced synaptic potentiation in both genotypes (Fig. 3*E*), which is consistent with previous reports (Stanton and Sarvey, 1985; two-way RM $ANOVA_{40\text{-}60min}$ time: $F_{(20,800)} = 1.05$, $p = 0.42$). Thus, β_1-ARs appear to be necessary for the enhanced synaptic potentiation at MPP–DCG synapses.

Biochemical measures partially detect heightened β-AR function in TgF344-AD rats

β-ARs are G-protein-coupled receptors, and both β_1 and β_2 couple to the G_S subtype, which triggers the activation of adenylate cyclase. Subsequently, cAMP-dependent protein kinase A (PKA) activation phosphorylates serine 845 (pSer845) on GluA1 subunits of AMPARs, leading to their insertion and the potentiation of synaptic transmission (Tran et al., 2004; Oh et al., 2006; O'Dell et al., 2015). β-AR activation also increases ERK1/2 (44/42 kDa, respectively) signaling downstream of Src kinase activation (Hagena et al., 2016). Via these pathways, β-AR activation with ISO can cause synaptic potentiation and enhance LTP (Dahl and Sarvey, 1990; O'Dell et al., 2015; Hagena et al., 2016). Importantly, both tetanic stimulation and β-AR facilitated LTP, and learning and memory require phosphorylation and insertion of AMPARs and an increase in pERK (English and Sweatt, 1997; Impey et al., 1998; Winder et al., 1999; Schiff et al., 2017).

We used Western blot analysis following stimulation of acute slices with 1 μM ISO to determine whether biochemical measures might also be able to detect heightened β-AR function in TgF344-AD rats. Using 1 μM ISO was critical to determine whether biochemical differences exist since the heightened synaptic potentiation at MPP–DGC synapses in TgF344-AD rats was masked at 10 μM ISO. Furthermore, to capture a rapid increase in pERK following β-AR activation, we exposed dissected sections of DG to ISO (1 μM) for 0, 30, 60, or 120 s. We measured pERK and total ERK in whole homogenates of isolated DG by Western blot and analyzed the ratio of pERK/total ERK versus untreated control (baseline) at the last time point (120 s). Consistent with 1 μM ISO being at threshold, we observed a significant increase in pERK42/total ERK42 at 120 s in TgF344-AD ($t_{(15)} = 2.59$, $p = 0.02$), but not in WT homogenates ($t_{(16)} = 0.85$, $p = 0.41$; Fig. 4*B2*). Furthermore, when viewing the result of each experiment plotted separately (Fig. 4*B2*), it can be seen that many more individual samples had an increase in pERK42/total ERK42 in homogenates from TgF344-AD rats ($n = 13/16$, ~81%) than WT rats ($n = 7/17$, ~41%), which is consistent with heightened β-AR function in TgF344-AD rats. pERK44/total ERK44 was also significantly increased in TgF344-AD DG homogenates ($t_{(15)} = 02.83$, $p = 0.012$; accounting for an increase of

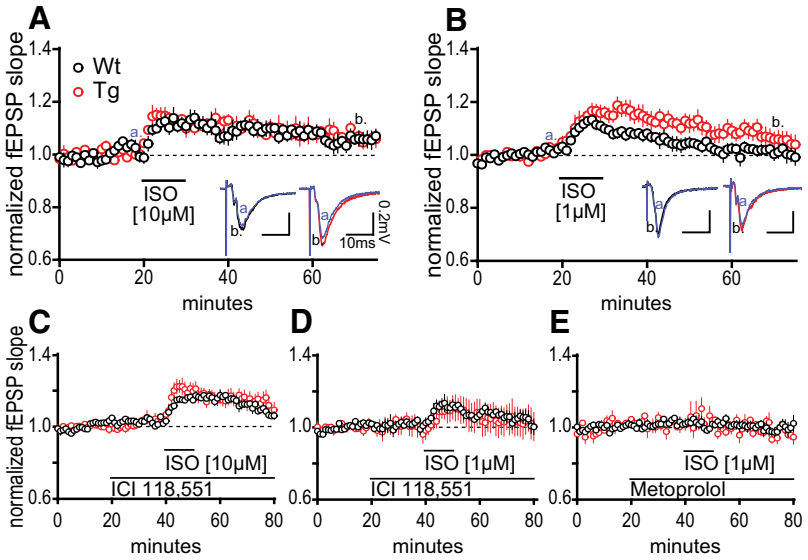

Figure 3. β-AR activation is sufficient to induce heightened synaptic potentiation at MPP–DGC synapses in TgF344-AD rats. ***A***, Bath application the β-AR selective agonist ISO (10 μM) elicits the same magnitude potentiation of the fEPSP at MPP–DGC synapses in both genotypes that returns to baseline by 40 min postwashout ($t_{(9)}$ = 0.0302, p = 0.9766; WT, n = 4; Tg, n = 6). Representative fEPSPs from WT (black) and Tg (red). Calibration: 0.2 mV, 10 mS (a = 20 min, b = 60 min). ***B***, ISO-induced increased synaptic potentiation at MPP–DGC synapses in Tg is revealed at a 1 μM concentration [non-WT (nWT) = 7; non-Tg (nTg) = 8]. Representative averaged fEPSP traces from WT (black) and Tg (red). Calibration: 0.2 mV, 10 ms (a = 20 min, b = 60 min). ***C***, ***D***, The β2-AR selective antagonist ICI 118,551 (300 nM) was ineffective at preventing the synaptic potentiation elicited at either 10 μM ISO (p < 0.01; WT, n = 4; Tg, n = 4; ***C***) or 1 μM ISO (p < 0.0001; ***D***; WT, n = 6; Tg, n = 4). ***E***, The β1-AR selective antagonist metoprolol (20 μM) completely prevented the synaptic potentiation in both genotypes induced by ISO (1 μM) stimulation (p > 0.1; WT, n = 3; Tg, n = 3). All data are from 9- to 10-month-old male Tg and WT rats, and values are the mean ± SEM.

32.1 ± 11.3%), but not in WT ($t_{(18)}$ = 1.29, p = 0.22; Fig. 4*B3*). Similar to pERK42/total ERK42, pERK44/total ERK44 was elevated in a larger fraction of samples from TgF344-AD rats (n = 13/16, ~81%) compared with WT rats (n = 10/19, ~53%).

Using the same protein samples, we asked whether there is a greater increase in pSer845-GluA1 downstream of β-AR and PKA activation in DG homogenates from TgF344-AD rats that could explain the heightened synaptic potentiation observed at MPP–DCG synapses. Again, at the 120 s time point, we found that pS845-GluA1 was increased by ISO exposure (p < 0.001), but we were unable to detect a difference between genotypes with Bonferroni correction as the increase also occurred in WT to the same degree ($t_{(23)}$ = 0.80, p > 0.99; Fig. 4*C*).

Activation of β-ARs increases the decay constant of voltage-gated calcium currents in TgF344-AD rat DGCs

β-ARs are also complexed with high-voltage-gated calcium channels (VGCCs) and PKA, and β-AR activation leads to phosphorylation of VGCCs, particularly L-type Ca^{2+} channels (Patriarchi et al., 2018) increasing open probability (Qian et al., 2017). To determine whether heightened β-AR function in TgF344-AD rats also enhances VGCC function, we compared peak current magnitude, total displaced charge, and decay time constant of Ca^{2+} currents recorded from voltage-clamped DGCs in response to voltage steps from −60 to +35 mV in slices from 9-month-old rats. To verify that there was no difference in the quality of the voltage control between groups, we evaluated the rise time of the Ca^{2+} currents with one-way ANOVA, which confirmed no differences ($F_{(1,74)}$ = 1.07, p = 0.37; Fig. 5*A*). Data were analyzed using two-way ANOVAs at peak charge displacement [holding potential (V_h) = −15 mV] for genotype and treatment, which was followed by one-tailed Bonferroni-corrected planned comparisons of treatment effect by genotype. To account for Ca^{2+} current rundown during whole-cell recordings (Murchison and Griffith, 1996), V_h step durations were shortened, resulting in a truncated Ca^{2+} current decay to baseline (Fig. 5*A*). To better represent the total charge displaced and to account for the truncated current, decay time (τ; in millisiemens) was calculated and compared.

We found no genotype difference in VGCC current amplitude (in picoamperes; $F_{(1,74)}$ = 0.25, p = 0.62) using a two-way ANOVA, but as expected, we found a significant effect of ISO treatment ($F_{(1,74)}$ = 12.71, p < 0.001). Planned comparisons using Bonferroni's correction revealed a significant effect of ISO exposure in WT ($t_{(74)}$ = 2.894, p = 0.0100), and a trend in TgF344-AD rats ($t_{(74)}$ = 2.083, p = 0.081; Fig. 5*C*). Importantly, there were no differences between genotypes without ISO exposure ($t_{(74)}$ = 0.46, p > 0.99), and the datapoints match perfectly when overlaid (Fig. 5*C*), demonstrating that the quality of the voltage clamp is shared between groups. Additional analysis reveals that charge displacement (picocoulombs) was not different between genotypes ($F_{(1,74)}$ = 0.07, p = 0.79) but was different by ISO treatment ($F_{(1,74)}$ = 16.63, p = 0.0001). Planned comparisons following Bonferroni's correction revealed a significant difference of ISO exposure in WT rats ($t_{(74)}$ = 3.118, p = 0.0052) and TgF344-AD rats ($t_{(74)}$ = 2.64, p = 0.020; Fig. 5*D*). Decay time was near the statistical cutoff between genotypes ($F_{(1,74)}$ = 3.41, p = 0.069), but was different by ISO treatment ($F_{(1,74)}$ = 7.67, p = 0.007). Planned comparisons using Bonferroni's correction revealed no significant difference between vehicle and ISO exposure in WT rats ($t_{(73)}$ = 0.86, p = 0.63), but a significant difference in TgF344-AD rats ($t_{(73)}$ = 3.47, p = 0.002), accounting for a 63.47 ± 18.3% increase in decay time in ISO (Fig. 5*F*,*G*). Together, these data suggest that heightened β-AR function in the DG of TgF344-AD rats is associated with enhanced decay times for VGCCs.

Enhanced LTP magnitude at MPP–DCG synapses in the TgF344-AD rat is dependent on heightened β-AR function

Our laboratory previously reported increased LTP magnitude induced by HFS at MPP–DGC synapses, but not at CA3–CA1 synapses at 6 months of age in TgF344-AD rats compared with WT rats (Smith and McMahon, 2018). Since activation of β-ARs facilitates LTP induction and increases LTP magnitude (Dahl and Sarvey, 1990; Dahl and Li, 1994; O'Dell et al., 2015; Hagena et al., 2016), we hypothesized that the heightened β-AR function might be responsible. To test this, we partially blocked β-ARs using a low concentration of the competitive β-AR antagonist PROP (3 μM) and induced LTP at MPP–DGC synapses in slices from TgF344-AD and WT rats. Because pharmacological inhibition of β-ARs can prevent LTP at MPP–DGC synapses in control animals (Swanson-Park et al., 1999; Hansen and Manahan-Vaughan, 2015), it was critical that the PROP concentration used had no effect on the LTP magnitude in WT rats. Recordings from TgF344-AD and WT rats were interleaved by

genotype and treatment (Fig. 6*A*,*B*). We confirmed that the strength of baseline transmission was not different between groups by averaging the final 5 min of the non-normalized fEPSP slope (in millivolts per millisecond; one-way ANOVA, $p > 0.05$). All experimental groups had significant LTP measured 40 min post-tetanus administration compared with baseline (paired *t* test, $p < 0.05$). However, LTP magnitude was significantly different between groups (one-way ANOVA: $F_{(3,\ 38)} = 4.192$, $p = 0.012$), with planned comparisons demonstrating that untreated TgF344-AD rats had a greater magnitude of LTP compared with WT rats ($q_{(38)} = 3.323$, $p = 0.006$), confirming our previous findings (Smith and McMahon, 2018). Importantly, 3 μM PROP had no effect on the magnitude of LTP in WT compared with untreated WT rats ($q_{(38)} = 0.488$, $p = 0.929$). Remarkably, partial blockade of β-ARs with 3 μM PROP completely restored the LTP magnitude in TgF344-AD rats to healthy WT levels ($q_{(38)} = 1.164$, $p = 0.518$; Fig. 6*A*).

To determine whether an even lower concentration of PROP is sufficient to reduce the magnitude of TgF344-AD rat LTP, we used 1 μM PROP and obtained the same results ($F_{(3,\ 37)} = 3.37$, $p = 0.029$). Specifically, untreated TgF344-AD rats had significantly heightened LTP compared with WT ($q_{(37)} = 2.506$, $p = 0.0439$), yet PROP-treated Tg and WT were not different (Tg_{PROP}: $q_{(37)} = 0.6017$, $p = 0.879$; WT_{PROP}: $q_{(37)} = 0.1699$, $p = 0.997$; Fig. 6*B*). Together, these data show that the heightened β-AR function causes the increased LTP magnitude at MPP–DGC synapses in TgF344-AD rats, providing a mechanistic explanation for the enhanced LTP.

We also previously reported heightened steady-state depolarization (SSD) at MPP–DGC synapses in TgF344-AD rats during administration of the tetanus used to induced LTP (Smith and McMahon, 2018). Therefore, we next sought to determine the role of heightened β-AR function on SSD after tetanus administration. SSD values were binned, normalized, and combined to permit statistical comparison (Fig. 6*C2*). The SSD was calculated by comparing the magnitude of the voltage deflection from baseline fEPSP once depolarization reaches steady state (determined via inflection point; Fig. 6*C1*). This value was found by square transforming the individual waveform and using an exponential curve fit ($y = ae^{bx}$), where the time and magnitude of the fEPSP are calculated. The time to reach SSD was the same between groups (one-way ANOVA: $F_{(3,80)} = 0.035$, $p = 0.99$; Fig. 6*C3*). However, significant group differences in the tetanus-induced SSD magnitude were detected ($F_{(3,80)} = 3.84$, $p = 0.014$). Specifically, while a Dunnett's test planned comparison demonstrated a significant increase in the SSD in untreated TgF344-AD rats compared with WT rats ($q_{(80)} = 2.928$, $p = 0.012$), there was no difference in the SSD magnitude between PROP-treated Tg and untreated WT rats ($q_{(80)} = 1.377$, $p = 0.379$), or PROP-treated WT ($q_{(80)} = 0.083$, $p = 0.999$) and untreated WT rats, recapitulating the LTP data (Fig. 6*C4*). These findings indicate that the heightened β-AR function contributes to the increase in tetanus-induced SSD in TgF344-AD rats.

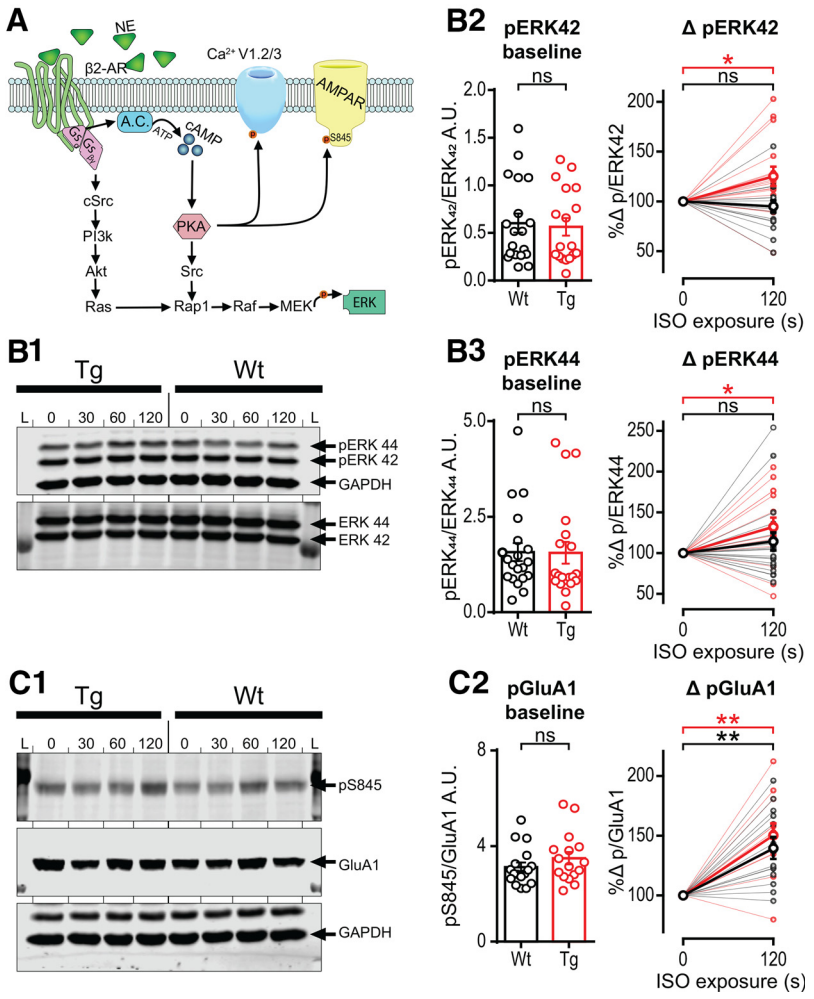

Figure 4. Phospho-ERK is enhanced in TgF344-AD rats with short-term ISO exposure, but phospho-GluA1 enhancement is not different between genotypes. ***A***, Representative schematic of canonical β_2-AR downstream cascade (Joiner et al., 2010; Hagena et al., 2016; Patriarchi et al., 2018). ***B1–B3***, Representative blots of phosphorylated ERK and total ERK. L, Ladder; 0, (no ISO exposure); 30, (30 s ISO) (1 μM) exposure; (60, 60 s ISO) (1 μM) exposure; (120, 120 s ISO) (1 μM) exposure. ***B1***, Representative blot of phospho-ERK44 and ERK42 with loading control GAPDH and total ERK. ***B2***, ***B3***, Individual samples from WT (black) and Tg (red) rats are not different at baseline (left bar chart) for either ERK42 (***B2***) or ERK44 (***B3***). The 120 s ISO exposure significantly increased pERK/total ERK (tERK; right scatter plot; thin lines represent individual samples; bold line represents averaged data) in Tg rats ($p < 0.05$), but not in WT rats ($p > 0.1$; ***B2***, right). The same was true for ERK44 in Tg rats ($p < 0.05$) and no increase in WT rats ($p > 0.1$; ***B3***, right). ***C1***, Representative blot of phosphorylated Ser845 on GluA1, total GluA1, and loading control GAPDH (see arrows). ***C2***, Individual samples from WT (black) and Tg (red) rats were not different at baseline (***C2***, left). Both genotypes had significantly enhanced pS845-GluA1 levels ($p < 0.001$), but there was no difference between genotypes ($p > 0.1$; thin lines represent individual samples; bold line represents averaged data). All data are from 9- to 10-month-old Tg ($n = 16$) and WT ($n = 17$) rats, and grouped values are the mean ± SEM. ns, not significant. *$p \leq 0.05$, **$p \leq 0.01$.

Enhanced sensitivity of β-ARs facilitates NOR and masks a cognitive deficit in extinction learning in TgF344-AD rats

Despite significant AD pathology and altered synaptic function beginning at 6 months of age in TgF344-AD rats (Cohen et al., 2013; Smith and McMahon, 2018), performance in hippocampus-dependent spatial tasks such as Morris water maze or Barnes maze is surprisingly not different from WT rats (Berkowitz et al., 2018; Pentkowski et al., 2018; Voorhees et al., 2018). At 9 months of age, reference memory in a T-maze is altered, but not working

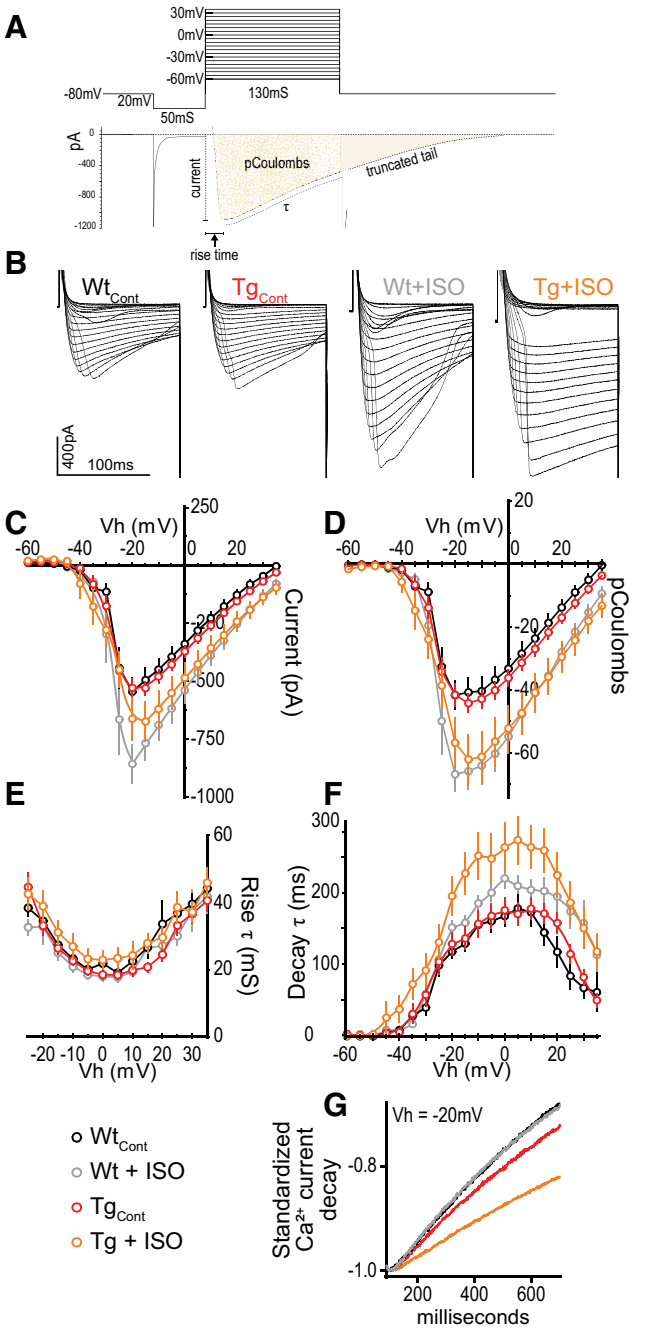

Figure 5. Activation of β-ARs slows the decay of voltage-gated calcium currents recorded from DGCs in TgF344-AD rats. ***A***, Illustration showing the voltage step protocol (top) and resulting VGCC (bottom) with relevant measures labeled. ***B***, Representative calcium currents from each voltage step between −60 and +35 mV from WT and Tg rats with or without ISO (1 μM) in the bath. Calibration: 400 pA,100 mS. ***C***, Graph of peak Ca^{2+} current (in picoamperes) showing no significant difference between genotypes under control conditions ($p > 0.1$), but was by ISO treatment ($p < 0.001$). ISO increased the current amplitude compared with control in WT rats ($p = 0.01$), but not in Tg rats ($p > 0.05$). ***D***, Total charge displacement (in picocoulombs) was not different by genotype ($p > 0.1$) but was different by ISO treatment ($p = 0.0001$). Analysis revealed a significant difference by ISO exposure in both WT rats ($p < 0.01$) and Tg rats ($p < 0.05$). ***E***, There was no difference in current rise time between groups ($p > 0.1$). ***F***, Decay time was not different between genotypes ($p > 0.05$) but was different by ISO treatment ($p < 0.01$). However, planned comparisons revealed a significant difference by ISO exposure in Tg rats ($p < 0.01$), accounting for an ~60% increase in decay time, in the absence of a difference in WT rats ($p > 0.1$). ***G***, Representative examples illustrating slower current decay following ISO exposure in recordings from Tg rats. All data from 9- to 10-month-old Tg and WT rats (WT: $n = 13$, $N = 6$; Tg: $n = 36$, $N = 15$; WT_{ISO}: $n = 12$, $N = 5$; Tg_{ISO}: $n = 17$, $N = 8$), and values are the mean ± SEM.

memory in a Y-maze (Tournier et al., 2020). Together, these data suggest that compensatory mechanisms must be maintaining function, but certain tasks may be more vulnerable to deterioration. β-ARs play a key role in memory acquisition and cognitive flexibility (Berridge and Waterhouse, 2003; Hagena et al., 2016), suggesting that heightened β-AR function might support performance in hippocampus-dependent tasks early in the disease. In fact, driving LC function through chemogenetic stimulation later in the disease abolished the deficit in spatial reversal learning in 16-month-old TgF344-AD rats (Rorabaugh et al., 2017). To determine whether memory and cognitive flexibility are reliant on the heightened β-AR function, we partially blocked them in two behavioral assays that depend on β-AR function (Kemp and Manahan-Vaughan, 2008; Sara, 2009; Do-Monte et al., 2010).

WT and TgF344-AD rats (10–11 months of age) were tested in a NOR task, as novelty is tightly associated with heightened LC function and requires β-AR function in hippocampus (Kemp and Manahan-Vaughan, 2008; Sara, 2009). All rats were implanted with cannulas in the lateral ventricles to deliver vehicle or PROP intracerebroventricularly 30 min before exposure to the arena each day (Fig. 7*A*). On day 1, all rats received a vehicle infusion and were acclimated to an empty arena for 5 min. On day 2, WT and TgF344-AD rats were randomly assigned and received either PROP [2 μg/animal, 1 μg/5 μl per hemisphere (as in the study by Kemp and Manahan-Vaughan, 2008)] or an equal volume of 0.9% saline vehicle before exposure to the arena containing two identical objects (Fig. 7*B*), where they were allowed to explore for 5 min. The purpose of PROP infusion on day 2 was to limit the involvement of β-AR activation on memory acquisition. On day 3, all rats received a vehicle infusion, and subsequently were placed into the arena that contained one familiar and one novel object and were allowed to explore for 5 min. The total distance traveled per group was compared across days with a two-way RM ANOVA showing a significant effect of day ($F_{(2, 154)} = 43.85$, $p < 0.0001$). Bonferroni-corrected multiple comparisons revealed a significant difference between vehicle-treated WT and TgF344-AD only on day 3 ($t_{(231)} = 2.460$, $p = 0.044$; Fig. 7*C*). A discrimination index (DI) was generated (time spent exploring novel object – time spent exploring familiar object divided by the total time spent exploring objects [(objN – objF)/objTotal]; Fig. 7*B*) to determine whether NOR occurred.

Before determining whether differences in NOR exist across treatment and genotype groups, we first asked whether there was significant NOR in each experimental group. To do this, we compared the discrimination index calculated on day 3 against chance (DI score = 0) using an independent-samples *t* test. Surprisingly, we found that vehicle-treated WT rats did not display significant NOR ($t_{(17)} = 0.044$, $p = 0.97$), while vehicle-treated TgF344-AD rats appeared to, with a *p* value just >0.05 ($t_{(10)} = 2.13$, $p = 0.059$, 95% CI = −0.017 to 0.79; Fig. 7*C*). Importantly, and in support of the hypothesis, when the TgF344-AD rats were treated with PROP, the discrimination index was not significantly different from chance ($t_{(11)} = 0.034$, $p = 0.97$), indicating that β-ARs must be driving the NOR displayed in the vehicle-treated TgF344-AD rats. When WT rats were treated with PROP, similar to vehicle-treated WT rats, the discrimination index was not different from chance, indicating a lack of NOR ($t_{(20)} = 0.27$, $p = 0.79$). Together, these data suggest that the heightened β-AR function facilitates NOR in TgF344-AD rats, similar to the heightened β-AR function driving enhanced LTP magnitude (Fig. 4). Of note, our finding of significant NOR in TgF344-AD rats

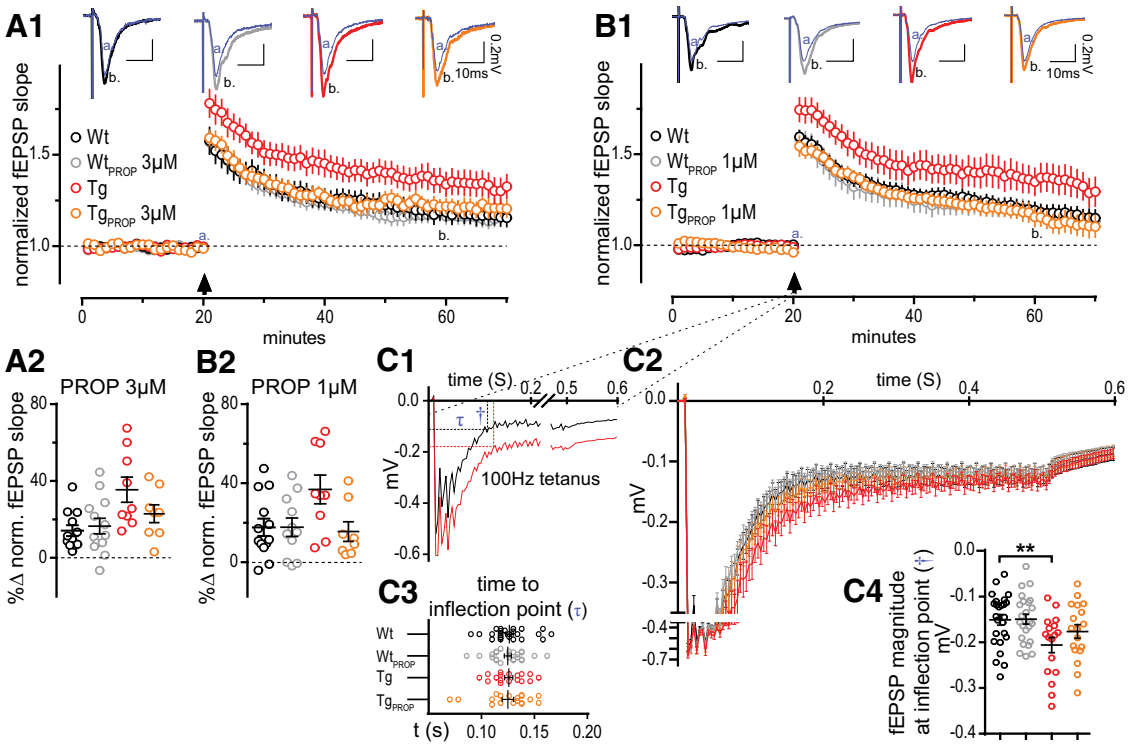

Figure 6. Heightened LTP at MPP–DGC synapse in the TgF344-AD rat is dependent on the enhanced function of β-ARs. ***A1***, Acute hippocampal slices from 6-month-old WT and Tg rats were recorded across the MPP–DGC synapses with or without a low dose of PROP (3 μM; WT, $n = 13$; WT_{PROP}, $n = 11$; Tg, $n = 9$; Tg_{PROP}, $n = 8$). ***B1***, Acute hippocampal slices from the same animals were run in parallel in which the concentration of PROP was threefold lower (1 μM). ***A1–B2***, Arrow, HFS was delivered after 20 min stable baseline. Baseline fEPSP slope *t*(a: 16–20 min) was compared against those 40 min post-tetanus administration *t*(b: 61–65 min). All groups successfully potentiated ($p < 0.05$). Prenormalized baseline values were not different between experimental groups in the (3 μM) or (1 μM) electrophysiology setup results ($p < 0.05$). ***A2***, Groups on the (3 μM) electrophysiology setup were different at time 60 (b; $p < 0.05$) with planned comparisons against the WT control, which was only different from Tg ($p < 0.01$), and not WT_{PROP} ($p > 0.1$) or Tg_{PROP} ($p > 0.1$; ***B2***) Groups on the 1 μM electrophysiology setup were different at time 60 (b; $p < 0.05$) with planned comparisons against the WT control, which was only different from Tg ($p < 0.05$), and not WT_{PROP} ($p > 0.1$) or Tg_{PROP} ($p > 0.1$). ***C1–C4***, Evaluation of steady-state depolarization (SSD) during tetanus. ***C1***, Representative fEPSPs during tetanus displaying the time to the inflection point (τ) and the magnitude of the depolarization (†) as calculated by curve fitting. ***C2***, Standardized and binned fEPSPs with stimulus artifacts removed were combined. ***C3***, No differences in the time to reach SSD ($p > 0.1$). ***C4***, Significant group differences were detected in the magnitude of the fEPSP at the inflection point ($p < 0.05$). Planned comparisons to WT control were not significant for WT_{PROP} ($p > 0.1$) or Tg_{PROP} ($p > 0.1$), but were significantly elevated for TgCont ($p < 0.05$). All grouped values are the mean ± SEM. $^{**}p \leq 0.01$.

but not in WT rats is reminiscent of significant NOR in 5XFAD mice but not in WT mice (Braun and Feinstein, 2019).

Next, the same cohort of WT and TgF344-AD rats, keeping the treatment groups as in NOR, underwent a contextual fear conditioning with a single learning trial followed by three extinction trials. Rats spent 7 min in a novel context and were shocked three times (0.5 mA, 1 s duration, 1 min interval) to induce fear learning before removal from the chamber (Fig. 7*A*,*E2*). To determine the effect of β-ARs on fear extinction learning, rats were infused with PROP or saline 30 min before being returned to the context/box for extinction learning on days 2, 3, and 4 without shock (Fig. 7*A*,*E3*). Time spent freezing was measured and compared. Although TgF344-AD rats spent significantly more time moving before shock at baseline, as determined by an unpaired *t* test with Welch correction for nonequal variance ($t_{(28.09)} = 2.67$, $p = 0.013$), there were no significant differences in fear memory (one-way ANOVA, percentage of freezing on day 2: $F_{(3, 58)} = 1.74$, $p = 0.17$; Fig. 7*E2*). A two-way RM ANOVA across days 2–4, with planned comparisons for the final fear extinction exposure on day 4, revealed a significant main effect of day ($F_{(2,114)} = 12.73$, $p < 0.0001$), but no interaction or main effect of treatment ($F_{(6,114)} = 0.1913$, $p = 0.1913$; $F_{(3,57)} = 2.144$, $p = 0.10$, respectively; Fig. 7*E*). Dunnett's corrected planned comparisons were made between each group versus WT control to assess normal fear extinction learning. Remarkably, only the TgF344-AD rats treated with PROP were significantly different on day 4 ($q_{(228)} = 3.879$, $p = 0.0004$), demonstrating that blocking β-ARs inhibits their ability to successfully learn fear extinction, resulting in 27.23% increase in freezing time compared with WT control rats. Importantly, PROP infusion in WT rats had no effect on their ability to extinguish the contextual fear response. Together, these results show a greater reliance on β-AR function in fear extinction learning in TgF344-AD rats.

Discussion

The TgF344-AD rat model with human mutations in the APP_{swe} and $PS1_{\Delta E9}$ genes (Cohen et al., 2013) has early endogenous pTau accumulation in LC and hippocampal NA axon degeneration during prodromal AD (Rorabaugh et al., 2017), recapitulating human AD (Booze et al., 1993; Gulyás et al., 2010; Braak et al., 2011). This pathology is unique to the TgF344-AD rat, making it a powerful preclinical model to reveal the consequences of NA system dysfunction on hippocampal synaptic physiology and learning and memory during the earliest phases of the disease. Excitatory inputs from the EC to DG dysfunction first in human AD (Khan et al., 2014) and also in TgF344-AD rats, where we reported decreased strength of basal excitatory transmission at MPP–DGC synapses before CA3–CA1 synapses, and heightened LTP magnitude only at MPP–DGC synapses (Smith and

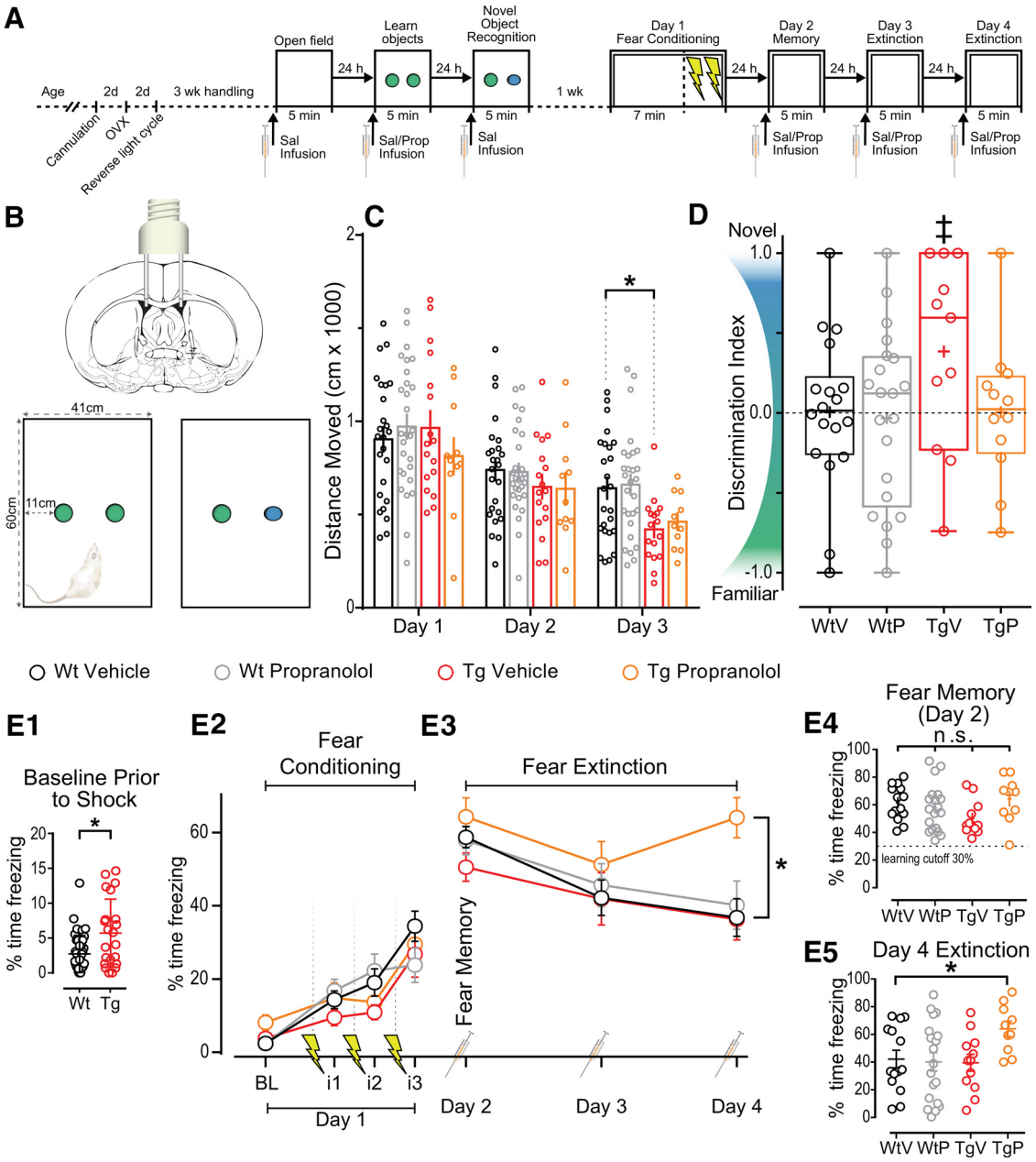

Figure 7. Enhanced function of β-ARs may provide gain of function for NOR and masks a cognitive deficit in extinction learning. ***A***, Representative schematic of behavioral assays and preparatory procedures. ***B***, Representative schematic of bilateral lateral ventricle infusion of rats and NOR box size and object distribution. ***C***, Total distance moved on days 1, 2, and 3 of NOR divided by group. Data show a significant effect of day ($p < 0.0001$). Planned comparisons demonstrate the only significant difference between groups by day is day 3 WtV and TgV ($p < 0.05$). ***D***, DI [(Nov − Fam)/Total] for each group (WtV, $n = 15$; WtP, $n = 17$; TgV, $n = 8$; TgP, $n = 7$). The discrimination index in each experimental group was independently compared against chance (DI=0) and reveals that TgV rats displayed significant NOR at the $p < 0.06$ level (‡). Other groups were not different from chance, each ($p > 0.1$; + for mean value and mid-line of box denotes median value). ***E1–E4***, Graphs of fear conditioning and fear extinction (WtV, $n = 22$; WtP, $n = 19$; TgV, $n = 11$; TgP, $n = 11$). ***E1***, Baseline freezing was assessed before shock to show significant differences in baseline freezing ($p < 0.05$). ***E2***, Graph of freezing during baseline (BL) and freezing during the 1 min interval (i) following each shock. ***E3***, Graph of day 2, day 3, and day 4 showing the steady reduction of freezing over time. Data show that, compared with WtV (control) levels, there was no significant difference of group ($p > 0.1$) but there was a significant effect of day ($p < 0.0001$). Planned comparisons show that only TgP was different from WtV on day 4 ($p < 0.01$) in which TgP spent 27.23% more time freezing. ***E4***, All groups learned the fear memory as determined via paired *t* tests ($p < 0.0001$). ***E5***, Individual data points from day 4 showing the distributions between groups. All grouped data show the mean ± SEM. ns, not significant. $^{*}p \leq 0.05$, $^{‡}p \leq 0.06$.

McMahon, 2018). Since β-AR activation increases synaptic plasticity at MPP–DGC synapses (Pelletier et al., 1994; Lethbridge et al., 2014; O'Dell et al., 2015; Hagena et al., 2016) and facilitates learning and memory (Hagena et al., 2016) in healthy animals, heightened β-AR function linked to AD pathology could maintain hippocampal function early in the disease, despite the increase in Aβ production (Ni et al., 2006). Here, we tested this hypothesis and report that significant loss of NA axons in hippocampus is associated with heightened β-AR-induced synaptic potentiation at MPP–DGC synapses, which drives the increase in LTP magnitude. Furthermore, we find that TgF344-AD rats are more reliant on β-ARs during extinction learning compared with WT rats and that β-ARs facilitate NOR in TgF344-AD rats. Thus, our findings are consistent with the interpretation that a compensatory increase in β-AR function, temporally linked with the loss of NA axons in hippocampus and

increased Aβ accumulation, enhances synaptic function that supports some forms of learning and memory during prodromal AD.

Initial investigation of the NA fiber density in TgF344-AD rats using immunohistochemical staining against the NE transporter showed reduced density at 16 months but not at 6 months (Rorabaugh et al., 2017). We expanded on these findings and report no genotype difference at 3 months of age but a modest yet significant reduction of TH^+ fiber density in TgF344-AD rats at 6 months of age. Although anti-TH immunohistochemistry will also identify dopaminergic axons, in hippocampus, LC NA axons are the major source of dopamine (Kempadoo et al., 2016), suggesting that the loss of TH^+ axons we observed originate primarily from the LC. Importantly, our finding of reduced TH^+ fiber density in hippocampus occurs precisely within the temporal window when pTau is first found in the LC (Rorabaugh et al., 2017), amyloid β deposits form in hippocampus (Fig. 1*A*, arrow; Rorabaugh et al., 2017), and heightened LTP occurs at MPP–DGC synapses (Smith and McMahon, 2018). These overlapping windows of pathology onset provide several potential mechanisms, which may account for reduced fiber density in hippocampus. pTau accumulation in the LC is associated with reduced synaptic connections between LC neurons and mitochondrial dysfunction, which is only present in pTau-bearing LC cells (Andrés-Benito et al., 2017), suggesting that afflicted cells may be unable to maintain the health of long-range axons in hippocampus. Also during this time frame, there is enhanced macrophage concentration in LC of TgF344-AD rats (Rorabaugh et al., 2017), which is consistent with the idea that immune responses to heightened inflammatory markers such as IL-1β seen in pTau containing human LC, may subject them to immune-triggered destruction (Andrés-Benito et al., 2017). In addition, P301S pTau containing TH^+ LC primary mouse cell cultures also contain truncated projections, highlighting the neurotoxic effects of pTau on neuron fibers (Rorabaugh et al., 2017). Alternatively, the accumulation of Aβ within hippocampus may create an environment not conducive to support the health of NA axons. Specifically, Aβ interacts with and downregulates neurotrophin receptors TrkA and $p75^{NTR}$ (Olivieri et al., 2002; Benilova et al., 2012; De Strooper and Karran, 2016) and NT-4/5 levels in hippocampus and cerebellum (Hock et al., 2000), which are important for LC cell survival (Friedman et al., 1993) and for stimulating neurite regrowth (Nelson et al., 2014). Because the TgF344-AD rats recapitulate many of the pathologic features in human AD, the mechanisms causing NA axon degeneration as the disease progresses might be important for future studies to investigate.

Enhanced LTP magnitude at MPP–DGC synapses was first reported in APP/PS1 transgenic mice more than a decade ago (Yoshiike et al., 2008), yet the mechanism driving this heightened plasticity has been unresolved. Here, we found that loss of hippocampal TH^+ axons in TgF344-AD rats beginning at 6 months of age is temporally associated with the heightened LTP magnitude at MPP–DGC synapses we previously reported (Smith and McMahon, 2018). Because pharmacological activation of β-ARs at MPP–DGC synapses enhance LTP magnitude in control conditions (Pelletier et al., 1994; Lethbridge et al., 2014; O'Dell et al., 2015; Hagena et al., 2016), and their activation can prevent acute neurotoxic inhibition of LTP by application of Aβ in acute rat MPP–DGC slices (Wang et al., 2009), we were prompted to test whether the heightened activity of β-ARs at MPP–DGC synapses could be driving the heightened LTP we previously reported. Remarkably, weak pharmacological inhibition of β-ARs using the selective antagonist, PROP, did not affect the LTP magnitude at MPP–DCG synapses in WT rats but eliminated the heightened LTP magnitude at MPP–DCG synapses in TgF344AD rats, restoring it to WT levels. It is important to note that dopamine also modulates LTP magnitude in hippocampus (Broussard et al., 2016; Papaleonidopoulos et al., 2018), and it is released by LC NA axons (Lim et al., 2010; Kempadoo et al., 2016). However, the restoration of LTP magnitude in TgF344-AD rats to the WT level confirms the role of NE rather than dopamine. Importantly, this compensatory mechanism may explain the enhanced MPP–DGC LTP magnitude reported previously in the B6.152H and APP/PS1 transgenic AD mouse models (Yoshiike et al., 2008; Poirier et al., 2010). It is also important to note that CA3–CA1 synapses contain far fewer β-ARs than MPP–DGC synapses, which likely explains our observed lack of heightened LTP magnitude at CA3–CA1 synapses in TgF344-AD rats (Smith and McMahon, 2018). Finally, LTP is reduced in the vast majority of transgenic AD mouse models (Selkoe, 2002; Koppensteiner et al., 2016; Mango et al., 2019), suggesting that β-AR function is not enhanced and the toxic effects of Aβ are prevailing. Thus, our results provide a cellular mechanism for an otherwise unexplained enhancement of LTP at MPP–DGC synapses.

One possible mechanism for the heightened β-AR function is upregulated expression, which occurs following denervation (Harro et al., 1999). However, the temporal association with Aβ accumulation and the known binding of Aβ to β_2-ARs that enhance their function could also explain the heightened β-AR function (Wang et al., 2010, 2011). It may be more likely that the heightened LTP magnitude is a consequence of increased receptor expression, since increased Aβ typically causes deficits in LTP (Rowan et al., 2003), not heightened LTP. Furthermore, β-ARs are also expressed by neuroglia and microvessels throughout the hippocampus and are thought to increase in number following LC denervation (Kalaria et al., 1989a,b). Because astrocytes can modulate synaptic plasticity (Henneberger et al., 2010; Adamsky et al., 2018), we cannot rule out a contribution of β-ARs on glia to the heightened LTP and behavioral effects in the TgF344-AD rat, and perhaps in AD patients as well. Clearly, additional studies are needed to determine the cellular and molecular mechanisms driving the heightened β-AR function.

Our finding of heightened β-AR function in TgF344-AD rats raises the question of their behavioral significance. Despite the significant pathology at 6–9 months of age and synaptic alterations (Smith and McMahon, 2018), many forms of learning and memory have been reported to be largely unaffected (Cohen et al., 2013; Rorabaugh et al., 2017; Berkowitz et al., 2018; Pentkowski et al., 2018; Voorhees et al., 2018), mimicking the preclinical or prodromal stage of AD in humans (Sperling et al., 2011). Consistent with our finding that heightened β-AR function causes heightened LTP magnitude, they also appear to facilitate NOR in TgF344-AD rats under conditions where there is no significant NOR in WT control rats. Importantly, our finding of facilitated NOR in TgF344-AD mirrors enhanced NOR in the 5xFAD mouse model (Braun and Feinstein, 2019), suggesting the possibility that heightened function of β-ARs is responsible for this behavioral advantage in the 5xFAD model as well. Moreover, partial blockade of β-ARs unmasked a deficit in fear extinction learning only in TgF344-AD rats, indicating a stronger

reliance on β-ARs for behavioral competency. This is an important finding since patients with aMCI and early AD have impaired fear extinction (Nasrouei et al., 2020). In the APP/PS1 and 3xTg mouse models, pharmacologically blocking β_2-ARs increased escape latency in the Morris water maze without affecting performance in WT rats (Branca et al., 2014; Wu et al., 2017), yet activating β_1-ARs in the 5xFAD model was deleterious (Ardestani et al., 2017). Clearly, β-ARs have important, yet underappreciated, roles in maintaining synaptic plasticity and some hippocampus-dependent behaviors in early stages of AD.

In conclusion, our results provide evidence of heightened β-AR function in a preclinical AD rat model that is temporally associated with loss of noradrenergic innervation and Aβ plaque deposition in hippocampus and pTau accumulation in LC (Rorabaugh et al., 2017). Importantly, heightened β-AR function is responsible for enhanced LTP at MPP–DGC synapses in TgF344-AD rats that may also explain increased LTP at these same synapses in some transgenic mouse models of AD (Yoshiike et al., 2008; Poirier et al., 2010). Finally, the heightened synaptic plasticity driven by increased function of β-ARs likely underlies the preservation of some types of learning and memory, which may have major implications for cognitive function in early phases of AD in patients.

References

Adamsky A, Kol A, Kreisel T, Doron A, Ozeri-Engelhard N, Melcer T, Refaeli R, Horn H, Regev L, Groysman M, London M, Goshen I (2018) Astrocytic activation generates de novo neuronal potentiation and memory enhancement. Cell 174:59–71.e14.

Andrés-Benito P, Fernández-Dueñas V, Carmona M, Escobar LA, Torrejón-Escribano B, Aso E, Ciruela F, Ferrer I (2017) Locus coeruleus at asymptomatic early and middle Braak stages of neurofibrillary tangle pathology. Neuropathol Appl Neurobiol 43:373–392.

Ardestani PM, Evans AK, Yi B, Nguyen T, Coutellier L, Shamloo M (2017) Modulation of neuroinflammation and pathology in the 5XFAD mouse model of Alzheimer's disease using a biased and selective beta-1 adrenergic receptor partial agonist. Neuropharmacology 116:371–386.

Arendt T, Brückner MK, Morawski M, Jäger C, Gertz H-J (2015) Early neurone loss in Alzheimer's disease: cortical or subcortical? Acta Neuropathol Commun 3:10.

Arganda-Carreras I, Kaynig V, Rueden C, Eliceiri KW, Schindelin J, Cardona A, Sebastian Seung H (2017) Trainable Weka Segmentation: a machine learning tool for microscopy pixel classification. Bioinformatics 33:2424–2426.

Bannister R, Boylston AW, Davies IB, Mathias CJ, Sever PS, Sudera D (1981) β-receptor numbers and thermodynamics in denervation supersensitivity. J Physiol 319:369–377.

Benilova I, Karran E, De Strooper B (2012) The toxic Aβ oligomer and Alzheimer's disease: an emperor in need of clothes. Nat Neurosci 15:349–357.

Berkowitz LE, Harvey RE, Drake E, Thompson SM, Clark BJ (2018) Progressive impairment of directional and spatially precise trajectories by TgF344-Alzheimer's disease rats in the Morris Water Task. Sci Rep 8:16153.

Berridge CW, Waterhouse BD (2003) The locus coeruleus-noradrenergic system: modulation of behavioral state and state-dependent cognitive processes. Brain Res Brain Res Rev 42:33–84.

Booze RM, Mactutus CF, Gutman CR, Davis JN (1993) Frequency analysis of catecholamine axonal morphology in human brain. II. Alzheimer's disease and hippocampal sympathetic ingrowth. J Neurol Sci 119:110–118.

Braak H, Thal DR, Ghebremedhin E, Del Tredici K (2011) Stages of the pathologic process in Alzheimer disease: age categories from 1 to 100 years. J Neuropathol Exp Neurol 70:960–969.

Branca C, Wisely EV, Hartman LK, Caccamo A, Oddo S (2014) Administration of a selective β2 adrenergic receptor antagonist exacerbates neuropathology and cognitive deficits in a mouse model of Alzheimer's disease. Neurobiol Aging 35:2726–2735.

Braun D, Feinstein DL (2019) The locus coeruleus neuroprotective drug vindeburnol normalizes behavior in the 5xFAD transgenic mouse model of Alzheimer's disease. Brain Res 1702:29–37.

Broussard JI, Yang K, Levine AT, Tsetsenis T, Jenson D, Cao F, Garcia I, Arenkiel BR, Zhou F-M, De Biasi M, Dani JA (2016) Dopamine regulates aversive contextual learning and associated in vivo synaptic plasticity in the hippocampus. Cell Rep 14:1930–1939.

Chiodo LA, Acheson AL, Zigmond MJ, Stricker EM (1983) Subtotal destruction of central noradrenergic projections increases the firing rate of locus coeruleus cells. Brain Res 264:123–126.

Cohen RM, Rezai-Zadeh K, Weitz TM, Rentsendorj A, Gate D, Spivak I, Bholat Y, Vasilevko V, Glabe CG, Breunig JJ, Rakic P, Davtyan H, Agadjanyan MG, Kepe V, Barrio JR, Bannykh S, Szekely CA, Pechnick RN, Town T (2013) A transgenic Alzheimer rat with plaques, tau pathology, behavioral impairment, oligomeric aβ, and frank neuronal loss. J Neurosci 33:6245–6256.

Coulter DA, Carlson GC (2007) Functional regulation of the dentate gyrus by GABA-mediated inhibition. Prog Brain Res 163:235–243.

Dahl D, Li J (1994) Induction of long-lasting potentiation by sequenced applications of isoproterenol. Neuroreport 5:657–660.

Dahl D, Sarvey JM (1990) Beta-adrenergic agonist-induced long-lasting synaptic modifications in hippocampal dentate gyrus require activation of NMDA receptors, but not electrical activation of afferents. Brain Res 526:347–350.

Deguchi T, Axelrod J (1973) Supersensitivity and subsensitivity of the beta-adrenergic receptor in pineal gland regulated by catecholamine transmitter. Proc Natl Acad Sci U S A 70:2411–2414.

Dengler CG, Coulter DA (2016) Normal and epilepsy-associated pathologic function of the dentate gyrus. Prog Brain Res 226:155–178.

De Strooper B, Karran E (2016) The cellular phase of Alzheimer's disease. Cell 164:603–615.

Do-Monte FHM, Kincheski GC, Pavesi E, Sordi R, Assreuy J, Carobrez AP (2010) Role of beta-adrenergic receptors in the ventromedial prefrontal cortex during contextual fear extinction in rats. Neurobiol Learn Mem 94:318–328.

Dooley DJ, Mogilnicka E, Delini-Stula A, Waechter F, Truog A, Wood J (1983) Functional supersensitivity to adrenergic agonists in the rat after DSP-4, a selective noradrenergic neurotoxin. Psychopharmacology (Berl) 81:1–5.

Doroshenko PA, Kostyuk PG, Martynyuk AE (1982) Intracellular metabolism of adenosine 3′,5′-cyclic monophosphate and calcium inward current in perfused neurones of Helix pomatia. Neuroscience 7:2125–2134.

English JD, Sweatt JD (1997) A requirement for the mitogen-activated protein kinase cascade in hippocampal long term potentiation. J Biol Chem 272:19103–19106.

Forest KH, Nichols RA (2019) Assessing neuroprotective agents for Aβ-induced neurotoxicity. Trends Mol Med 25:685–695.

Friedman WJ, Ibáñez CF, Hallböök F, Persson H, Cain LD, Dreyfus CF, Black IB (1993) Differential actions of neurotrophins in the locus coeruleus and basal forebrain. Exp Neurol 119:72–78.

Gibbs ME, Summers RJ (2002) Role of adrenoceptor subtypes in memory consolidation. Prog Neurobiol 67:345–391.

Gulyás B, Brockschnieder D, Nag S, Pavlova E, Kása P, Beliczai Z, Légrádi A, Gulya K, Thiele A, Dyrks T, Halldin C (2010) The norepinephrine transporter (NET) radioligand (S,S)-[18F]FMeNER-D2 shows significant decreases in NET density in the human brain in Alzheimer's disease: a post-mortem autoradiographic study. Neurochem Int 56:789–798.

Hagena H, Hansen N, Manahan-Vaughan D β (2016) Adrenergic control of hippocampal function: subserving the choreography of synaptic information storage and memory. Cereb Cortex 26:1349–1364.

Hansen N (2017) The longevity of hippocampus-dependent memory is orchestrated by the locus coeruleus-noradrenergic system. Neural Plast 2017:2727602.

Hansen N, Manahan-Vaughan D (2015) Hippocampal long-term potentiation that is elicited by perforant path stimulation or that occurs in conjunction with spatial learning is tightly controlled by beta-adrenoreceptors and the locus coeruleus. Hippocampus 25:1285–1298.

Harro J, Pähkla R, Modiri A-R, Harro M, Kask A, Oreland L (1999) Dose-dependent effects of noradrenergic denervation by DSP-4 treatment on forced swimming and beta-adrenoceptor binding in the rat. J Neural Transm (Vienna) 106:619–629.

Heneka MT, Galea E, Gavriluyk V, Dumitrescu-Ozimek L, Daeschner J, O'Banion MK, Weinberg G, Klockgether T, Feinstein DL (2002) Noradrenergic depletion potentiates β-amyloid-induced cortical inflammation: implications for Alzheimer's disease. J Neurosci 22:2434–2442.

Heneka MT, Ramanathan M, Jacobs AH, Dumitrescu-Ozimek L, Bilkei-Gorzo A, Debeir T, Sastre M, Galldiks N, Zimmer A, Hoehn M, Heiss W-D, Klockgether T, Staufenbiel M (2006) Locus ceruleus degeneration promotes Alzheimer pathogenesis in amyloid precursor protein 23 transgenic mice. J Neurosci 26:1343–1354.

Henneberger C, Papouin T, Oliet SHR, Rusakov DA (2010) Long-term potentiation depends on release of D-serine from astrocytes. Nature 463:232–236.

Herrmann N, Lanctôt KL, Khan LR (2004) The role of norepinephrine in the behavioral and psychological symptoms of dementia. J Neuropsychiatry Clin Neurosci 16:261–276.

Hock C, Heese K, Hulette C, Rosenberg C, Otten U (2000) Region-specific neurotrophin imbalances in Alzheimer disease: decreased levels of brain-derived neurotrophic factor and increased levels of nerve growth factor in hippocampus and cortical areas. Arch Neurol 57:846–851.

Impey S, Obrietan K, Wong ST, Poser S, Yano S, Wayman G, Deloulme JC, Chan G, Storm DR (1998) Cross talk between ERK and PKA is required for Ca2+ stimulation of CREB-dependent transcription and ERK nuclear translocation. Neuron 21:869–883.

Jardanhazi-Kurutz D, Kummer MP, Terwel D, Vogel K, Dyrks T, Thiele A, Heneka MT (2010) Induced LC degeneration in APP/PS1 transgenic mice accelerates early cerebral amyloidosis and cognitive deficits. Neurochem Int 57:375–382.

Jardanhazi-Kurutz D, Kummer MP, Terwel D, Vogel K, Thiele A, Heneka MT (2011) Distinct adrenergic system changes and neuroinflammation in response to induced locus ceruleus degeneration in APP/PS1 transgenic mice. Neuroscience 176:396–407.

Joiner M-l. A, Lisé M-F, Yuen EY, Kam AYF, Zhang M, Hall DD, Malik ZA, Qian H, Chen Y, Ulrich JD, Burette AC, Weinberg RJ, Law P-Y, El-Husseini A, Yan Z, Hell JW (2010) Assembly of a beta2-adrenergic receptor–GluR1 signalling complex for localized cAMP signalling. EMBO J 29:482–495.

Kalaria RN, Andorn AC, Tabaton M, Whitehouse PJ, Harik SI, Unnerstall JR (1989a) Adrenergic receptors in aging and Alzheimer's disease: increased β_2-receptors in prefrontal cortex and hippocampus. J Neurochem 53:1772–1781.

Kalaria RN, Stockmeier CA, Harik SI (1989b) Brain microvessels are innervated by locus ceruleus noradrenergic neurons. Neurosci Lett 97:203–208.

Kelly SC, He B, Perez SE, Ginsberg SD, Mufson EJ, Counts SE (2017) Locus coeruleus cellular and molecular pathology during the progression of Alzheimer's disease. Acta Neuropathol Commun 5:8.

Kemp A, Manahan-Vaughan D (2008) Beta-adrenoreceptors comprise a critical element in learning-facilitated long-term plasticity. Cereb Cortex 18:1326–1334.

Kempadoo KA, Mosharov EV, Choi SJ, Sulzer D, Kandel ER (2016) Dopamine release from the locus coeruleus to the dorsal hippocampus promotes spatial learning and memory. Proc Natl Acad Sci U S A 113:14835–14840.

Khan UA, Liu L, Provenzano FA, Berman DE, Profaci CP, Sloan R, Mayeux R, Duff KE, Small SA (2014) Molecular drivers and cortical spread of lateral entorhinal cortex dysfunction in preclinical Alzheimer's disease. Nat Neurosci 17:304–311.

Koppensteiner P, Trinchese F, Fà M, Puzzo D, Gulisano W, Yan S, Poussin A, Liu S, Orozco I, Dale E, Teich AF, Palmeri A, Ninan I, Boehm S, Arancio O (2016) Time-dependent reversal of synaptic plasticity induced by physiological concentrations of oligomeric Aβ42: an early index of Alzheimer's disease. Sci Rep 6:32553.

Lethbridge RL, Walling SG, Harley CW (2014) Modulation of the perforant path-evoked potential in dentate gyrus as a function of intrahippocampal β-adrenoceptor agonist concentration in urethane-anesthetized rat. Brain Behav 4:95–103.

Lim EP, Tan CH, Jay TM, Dawe GS (2010) Locus coeruleus stimulation and noradrenergic modulation of hippocampo-prefrontal cortex long-term potentiation. Int J Neuropsychopharmacol 13:1219–1231.

Loy R, Koziell DA, Lindsey JD, Moore RY (1980) Noradrenergic innervation of the adult rat hippocampal formation. J Comp Neurol 189:699–710.

Mango D, Saidi A, Cisale GY, Feligioni M, Corbo M, Nisticò R (2019) Targeting synaptic plasticity in experimental models of Alzheimer's disease. Front Pharmacol 10:778.

McNaughton BL, Barnes CA (1977) Physiological identification and analysis of dentate granule cell responses to stimulation of the medial and lateral perforant pathways in the rat. J Comp Neurol 175:439–454.

Monti JM, D'Angelo L, Jantos H, Barbeito L, Abó V (1988) Effect of DSP-4, a noradrenergic neurotoxin, on sleep and wakefulness and sensitivity to drugs acting on adrenergic receptors in the rat. Sleep 11:370–377.

Moudy AM, Kunkel DD, Schwartzkroin PA (1993) Development of dopamine-beta-hydroxylase-positive fiber innervation of the rat hippocampus. Synapse 15:307–318.

Murchison D, Griffith WH (1996) High-voltage-activated calcium currents in basal forebrain neurons during aging. J Neurophysiol 76:158–174.

Nasrouei S, Rattel JA, Liedlgruber M, Marksteiner J, Wilhelm FH (2020) Fear acquisition and extinction deficits in amnestic mild cognitive impairment and early Alzheimer's disease. Neurobiol Aging 87:26–34.

Nelson AR, Kolasa K, McMahon LL (2014) Noradrenergic sympathetic sprouting and cholinergic reinnervation maintains non-amyloidogenic processing of AβPP. J Alzheimers Dis 38:867–879.

Ni Y, Zhao X, Bao G, Zou L, Teng L, Wang Z, Song M, Xiong J, Bai Y, Pei G (2006) Activation of β_2-adrenergic receptor stimulates γ-secretase activity and accelerates amyloid plaque formation. Nat Med 12:1390–1396.

Nicholas AP, Pieribone VA, Hökfelt T (1993) Cellular localization of messenger RNA for beta-1 and beta-2 adrenergic receptors in rat brain: an in situ hybridization study. Neuroscience 56:1023–1039.

O'Dell TJ, Connor SA, Guglietta R, Nguyen PV (2015) β-Adrenergic receptor signaling and modulation of long-term potentiation in the mammalian hippocampus. Learn Mem 22:461–471.

Oh MC, Derkach VA, Guire ES, Soderling TR (2006) Extrasynaptic membrane trafficking regulated by GluR1 serine 845 phosphorylation primes AMPA receptors for long-term potentiation. J Biol Chem 281:752–758.

Olivieri G, Novakovic M, Savaskan E, Meier F, Baysang G, Brockhaus M, Müller-Spahn F (2002) The effects of beta-estradiol on SHSY5Y neuroblastoma cells during heavy metal induced oxidative stress, neurotoxicity and beta-amyloid secretion. Neuroscience 113:849–855.

Papaleonidopoulos V, Kouvaros S, Papatheodoropoulos C (2018) Effects of endogenous and exogenous D1/D5 dopamine receptor activation on LTP in ventral and dorsal CA1 hippocampal synapses. Synapse 72:e22033.

Patriarchi T, Buonarati OR, Hell JW (2018) Postsynaptic localization and regulation of AMPA receptors and Cav1.2 by β2 adrenergic receptor/PKA and Ca^{2+}/CaMKII signaling. EMBO J 37:e99771.

Patrylo PR, Williamson A (2007) The effects of aging on dentate circuitry and function. In: The dentate gyrus: a comprehensive guide to structure, function, and clinical implications (Scharfman HE, ed), pp 679–696. Amsterdam: Elsevier.

Pelletier MR, Kirkby RD, Jones SJ, Corcoran ME (1994) Pathway specificity of noradrenergic plasticity in the dentate gyrus. Hippocampus 4:181–188.

Pentkowski NS, Berkowitz LE, Thompson SM, Drake EN, Olguin CR, Clark BJ (2018) Anxiety-like behavior as an early endophenotype in the TgF344-AD rat model of Alzheimer's disease. Neurobiol Aging 61:169–176.

Poe GR, Foote S, Eschenko O, Johansen JP, Bouret S, Aston-Jones G, Harley CW, Manahan-Vaughan D, Weinshenker D, Valentino R, Berridge C, Chandler DJ, Waterhouse B, Sara SJ (2020) Locus coeruleus: a new look at the blue spot. Nat Rev Neurosci 21:644–659.

Poirier R, Veltman I, Pflimlin MC, Knoflach F, Metzger F (2010) Enhanced dentate gyrus synaptic plasticity but reduced neurogenesis in a mouse model of amyloidosis. Neurobiol Dis 40:386–393.

Pugh PL, Vidgeon-Hart MP, Ashmeade T, Culbert AA, Seymour Z, Perren MJ, Joyce F, Bate ST, Babin A, Virley DJ, Richardson JC, Upton N, Sunter D (2007) Repeated administration of the noradrenergic neurotoxin *N*-(2-chloroethyl)-*N*-ethyl-2-bromobenzylamine (DSP-4) modulates neuroinflammation and amyloid plaque load in mice bearing amyloid precursor protein and presenilin-1 mutant transgenes. J Neuroinflammation 4:8.

Qian H, Patriarchi T, Price JL, Matt L, Lee B, Nieves-Cintrón M (2017) Phosphorylation of Ser1928 mediates the enhanced activity of the L-type Ca2+ channel Cav1.2 by the β2-adrenergic receptor in neurons. Sci Signal 10:eaaf9659.

Rey NL, Jardanhazi-Kurutz D, Terwel D, Kummer MP, Jourdan F, Didier A, Heneka MT (2012) Locus coeruleus degeneration exacerbates olfactory deficits in APP/PS1 transgenic mice. Neurobiol Aging 33:426.e1–11.

Rorabaugh JM, Chalermpalanupap T, Botz-Zapp CA, Fu VM, Lembeck NA, Cohen RM, Weinshenker D (2017) Chemogenetic locus coeruleus activation restores reversal learning in a rat model of Alzheimer's disease. Brain 140:3023–3038.

Rowan MJ, Klyubin I, Cullen WK, Anwyl R (2003) Synaptic plasticity in animal models of early Alzheimer's disease. Phil Trans R Soc Lond B 358:821–828.

Sara SJ (2009) The locus coeruleus and noradrenergic modulation of cognition. Nat Rev Neurosci 10:211–223.

Schiff HC, Johansen JP, Hou M, Bush DEA, Smith EK, Klein JE, LeDoux JE, Sears RM (2017) β-Adrenergic receptors regulate the acquisition and consolidation phases of aversive memory formation through distinct, temporally regulated signaling pathways. Neuropsychopharmacology 42:895–903.

Schindelin J, Arganda-Carreras I, Frise E, Kaynig V, Longair M, Pietzsch T, Preibisch S, Rueden C, Saalfeld S, Schmid B, Tinevez J-Y, White DJ, Hartenstein V, Eliceiri K, Tomancak P, Cardona A (2012) Fiji: an open-source platform for biological-image analysis. Nat Methods 9:676–682.

Selkoe DJ (2002) Alzheimer's disease is a synaptic failure. Science 298:789–791.

Smith LA, McMahon LL (2018) Deficits in synaptic function occur at medial perforant path-dentate granule cell synapses prior to Schaffer collateral-CA1 pyramidal cell synapses in the novel TgF344-Alzheimer's disease rat model. Neurobiol Dis 110:166–179.

Sperling RA, Aisen PS, Beckett LA, Bennett DA, Craft S, Fagan AM, Iwatsubo T, Jack CR, Kaye J, Montine TJ, Park DC, Reiman EM, Rowe CC, Siemers E, Stern Y, Yaffe K, Carrillo MC, Thies B, Morrison-Bogorad M, Wagster MV, et al (2011) Toward defining the preclinical stages of Alzheimer's disease: recommendations from the National Institute on Aging-Alzheimer's Association workgroups on diagnostic guidelines for Alzheimer's disease. Alzheimers Dement 7:280–292.

Stanton PK, Sarvey JM (1985) Blockade of norepinephrine-induced long-lasting potentiation in the hippocampal dentate gyrus by an inhibitor of protein synthesis. Brain Res 361:276–283.

Swaminath G, Xiang Y, Lee TW, Steenhuis J, Parnot C, Kobilka BK (2004) Sequential binding of agonists to the beta2 adrenoceptor. Kinetic evidence for intermediate conformational states. J Biol Chem 279:686–691.

Swanson-Park JL, Coussens CM, Mason-Parker SE, Raymond CR, Hargreaves EL, Dragunow M, Cohen AS, Abraham WC (1999) A double dissociation within the hippocampus of dopamine D1/D5 receptor and β-adrenergic receptor contributions to the persistence of long-term potentiation. Neuroscience 92:485–497.

Theofilas P, Ehrenberg AJ, Dunlop S, Di Lorenzo Alho AT, Nguy A, Leite REP, Rodriguez RD, Mejia MB, Suemoto CK, Ferretti-Rebustini REDL, Polichiso L, Nascimento CF, Seeley WW, Nitrini R, Pasqualucci CA, Jacob Filho W, Rueb U, Neuhaus J, Heinsen H, Grinberg LT (2017) Locus coeruleus volume and cell population changes during Alzheimer's disease progression: a stereological study in human postmortem brains with potential implication for early-stage biomarker discovery. Alzheimers Dement 13:236–246.

Theofilas P, Ehrenberg AJ, Nguy A, Thackrey JM, Dunlop S, Mejia MB, Alho AT, Paraizo Leite RE, Rodriguez RD, Suemoto CK, Nascimento CF, Chin M, Medina-Cleghorn D, Cuervo AM, Arkin M, Seeley WW, Miller BL, Nitrini R, Pasqualucci CA, Filho WJ, Rueb U, Neuhaus J, Heinsen H, Grinberg LT (2018) Probing the correlation of neuronal loss, neurofibrillary tangles, and cell death markers across the Alzheimer's disease Braak stages: a quantitative study in humans. Neurobiol Aging 61:1–12.

Tournier BB, Barca C, Fall AB, Gloria Y, Meyer L, Ceyzériat K (2020) Spatial reference learning deficits in absence of dysfunctional working memory in the TgF344-AD rat model of Alzheimer's disease. Genes Brain Behav. Advance online publication. Retrieved May 5, 2021. .

Tran TM, Friedman J, Qunaibi E, Baameur F, Moore RH, Clark RB (2004) Characterization of agonist stimulation of cAMP-dependent protein kinase and G protein-coupled receptor kinase phosphorylation of the beta2-adrenergic receptor using phosphoserine-specific antibodies. Mol Pharmacol 65:196–206.

Voorhees JR, Remy MT, Cintrón-Pérez CJ, El Rassi E, Khan MZ, Dutca LM, Yin TC, McDaniel LN, Williams NS, Brat DJ, Pieper AA (2018) (-)-P7C3-S243 protects a rat model of Alzheimer's disease from neuropsychiatric deficits and neurodegeneration without altering amyloid deposition or reactive glia. Biol Psychiatry 84:488–498.

Wang D, Govindaiah G, Liu R, De Arcangelis V, Cox CL, Xiang YK (2010) Binding of amyloid β peptide to β_2 adrenergic receptor induces PKA-dependent AMPA receptor hyperactivity. FASEB J 24:3511–3521.

Wang D, Yuen EY, Zhou Y, Yan Z, Xiang YK (2011) Amyloid beta peptide-(1-42) induces internalization and degradation of beta2 adrenergic receptors in prefrontal cortical neurons. J Biol Chem 286:31852–31863.

Wang Q-W, Rowan MJ, Anwyl R (2009) Inhibition of LTP by beta-amyloid is prevented by activation of beta2 adrenoceptors and stimulation of the cAMP/PKA signalling pathway. Neurobiol Aging 30:1608–1613.

Winder DG, Martin KC, Muzzio IA, Rohrer D, Chruscinski A, Kobilka B, Kandel ER (1999) ERK plays a regulatory role in induction of LTP by theta frequency stimulation and its modulation by β-adrenergic receptors. Neuron 24:715–726.

Wu Q, Sun J-x, Song X-h, Wang J, Xiong C-q, Teng F-x, Gao C-x (2017) Blocking beta 2-adrenergic receptor inhibits dendrite ramification in a mouse model of Alzheimer's disease. Neural Regen Res 12:1499–1506.

Yoshiike Y, Kimura T, Yamashita S, Furudate H, Mizoroki T, Murayama M, Takashima A (2008) GABA(A) receptor-mediated acceleration of aging-associated memory decline in APP/PS1 mice and its pharmacological treatment by picrotoxin. PLoS One 3:e3029.